# The Laser Interferometer System for the Large Optics Diamond Turning Machine
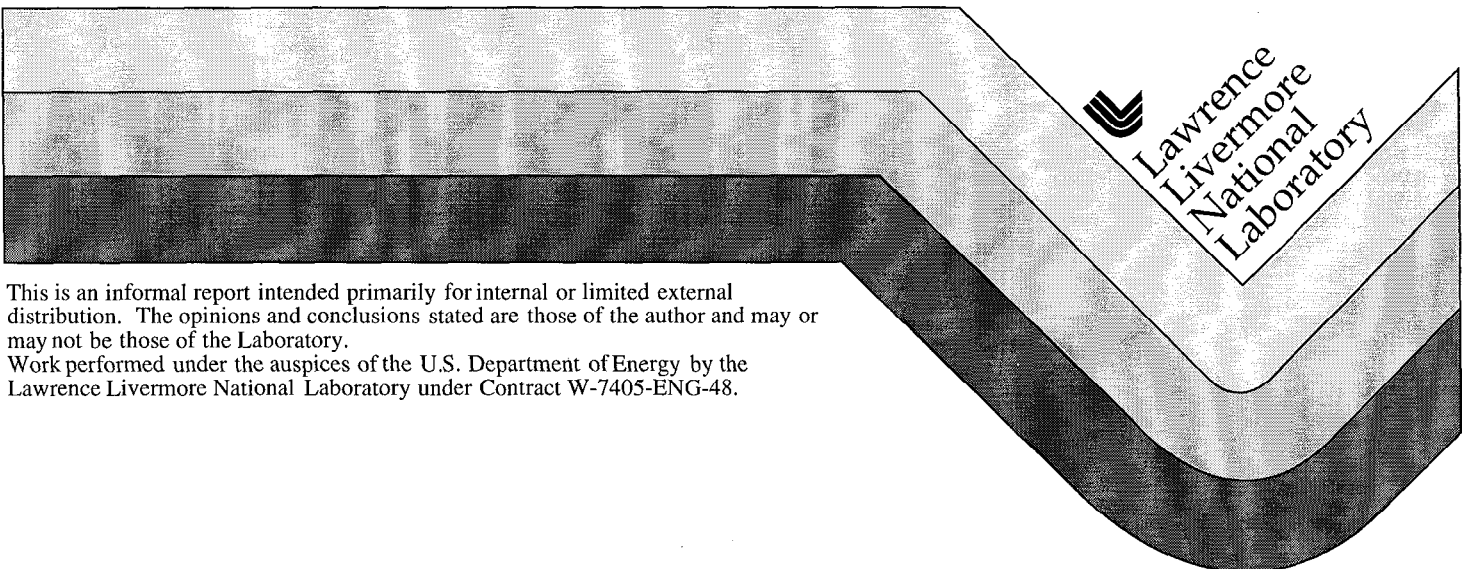
E.D. Baird
S.R. Patterson
R.R. Donaldson

**June 29, 1999**

DISCLAIMER

# THE LASER INTERFEROMETER SYSTEM
# FOR THE
# LARGE OPTICS DIAMOND TURNING MACHINE

**E.D. BAIRD**

**S.R. PATTERSON**

**R.R. DONALDSON**

**LAWRENCE LIVERMORE NATIONAL LABORATORY**

# ABSTRACT

# 1. INTRODUCTION AND OVERVIEW

The purpose of this report is to describe the Laser Interferometer System designed for the Large Optics Diamond Turning Machine (LODTM). To better understand the laser interferometer system, it is useful to begin with an overview of the LODTM metrology system.

The performance of the LODTM depends upon a highly accurate measurement of the position of the tool tip relative to the spindle faceplate. The set of components providing this information is referred to as the metrology system, and is depicted in Fig. 1. The metrology system uses a combination of stable structural elements, laser interferometers and capacitance gages to provide the necessary X axis and Z axis position information.

A principal feature of this system is the metrology frame, which is the origin or frame of reference for all measurements. To function as a reference, the metrology frame must be maintained at a constant size and shape. Therefore, the metrology frame is an independent structure that is kinematically supported on the LODTM main-frame by three blade flexures. Since it is isolated from variable loads, such as the moving machine slides or the workpiece weight, the metrology frame does not deform during machine operation. To avoid thermally induced size changes, the metrology frame is constructed of superinvar and is surrounded by hollow panels that are internally conditioned by temperature-controlled flowing water.

The layout of the interferometer measurement paths is depicted schematically in Fig. 2. Horizontal travel of the toolbar is measured by four laser interferometers that are arranged in left-right pairs at two different heights. The base of each interferometer is mounted on the metrology frame, and the measurements are made to vertical Zerodur straightedges mounted on opposite sides of the toolbar. With the aid of extensible metal bellows and glass windows, the interferometer and the beam paths are in a vacuum, except for small air gaps between the windows and the straightedges. The straightedges are kinematically mounted to the toolbar by flexures at two locations, and position measurements are made at two heights on each straightedge. This allows the horizontal (X) position of each lower straightedge mount to be calculated by the control system computers, independent of possible deformations due to loads on the toolbar.
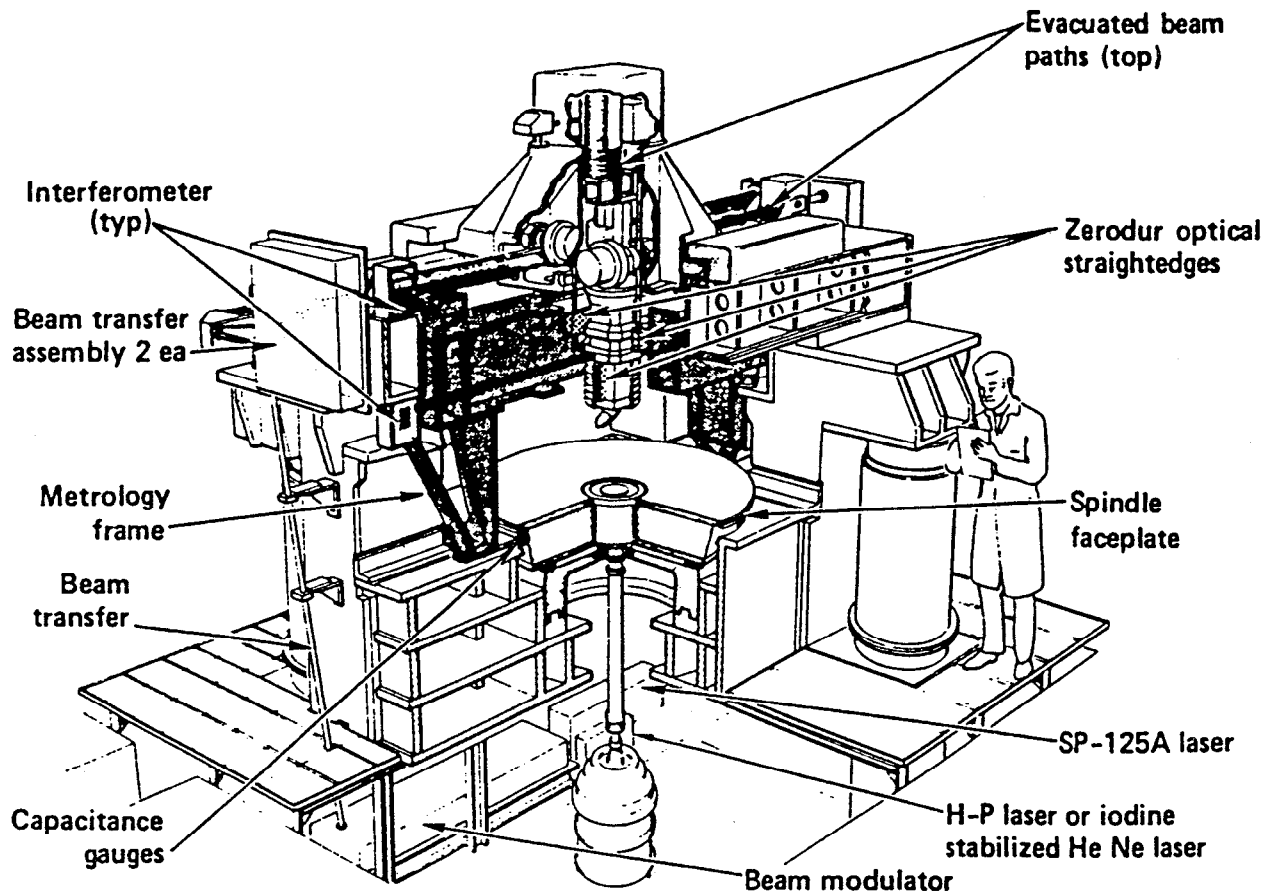
Figure 3.1  Location of the major components in the LODTM metrology system.

Symmetrical measurements are made on both sides of the toolbar in order to cancel some systematic errors by averaging the two measurements at each height, such as symmetric expansion of the metrology frame or the toolbar. Moreover, these redundant measurements allow the stability of the machine to be determined during use.

Vertical motion of the toolbar, relative to the metrology frame, is measured with three laser interferometers located in a Y-Z plane at the toolbar centerline. These interferometers are all mounted on a superinvar platform that is kinematically mounted inside of an evacuated box that is attached to the carriage above the toolbar. As before, the beam paths are evacuated. The center interferometer measures the vertical motion of a plane mirror mounted at the bottom of the hollow toolbar. The other two interferometers measure to the top surfaces of Zerodur straightedges that are attached to the metrology frame on either side of the toolbar centerline. The control computer subtracts the average of the latter two measurements from the center measurement, thereby cancelling any height change or roll motion of the carriage-mounted interferometer platform, and referencing the Z position of the toolbar to the metrology frame.

Although size and shape changes of the metrology frame are avoided, it can undergo small rigid-body movements during machine operation. These occur because the metrology frame is supported by the steel main-frame, which deforms by hundreds of microinches from weight shift of the moving slides, temperature disturbances, and other causes. To correct for the effects of such motion, and as well for motion within the spindle assembly, the motion of the metrology frame relative to the spindle faceplate is measured. These measurements, shown as Z3, Z4, X5, and X6 in Fig. 2, are made with double-sided capacitance gages mounted on the metrology frame that measure against rectangular grooves located near the outside of the spindle faceplate. It is then possible to show that small translations or rotations of the metrology frame in the X-Z plane produce self-cancelling signals in the interferometer and capacitance gage systems during the calculation of the toolbar-to-faceplate position by the control computer.
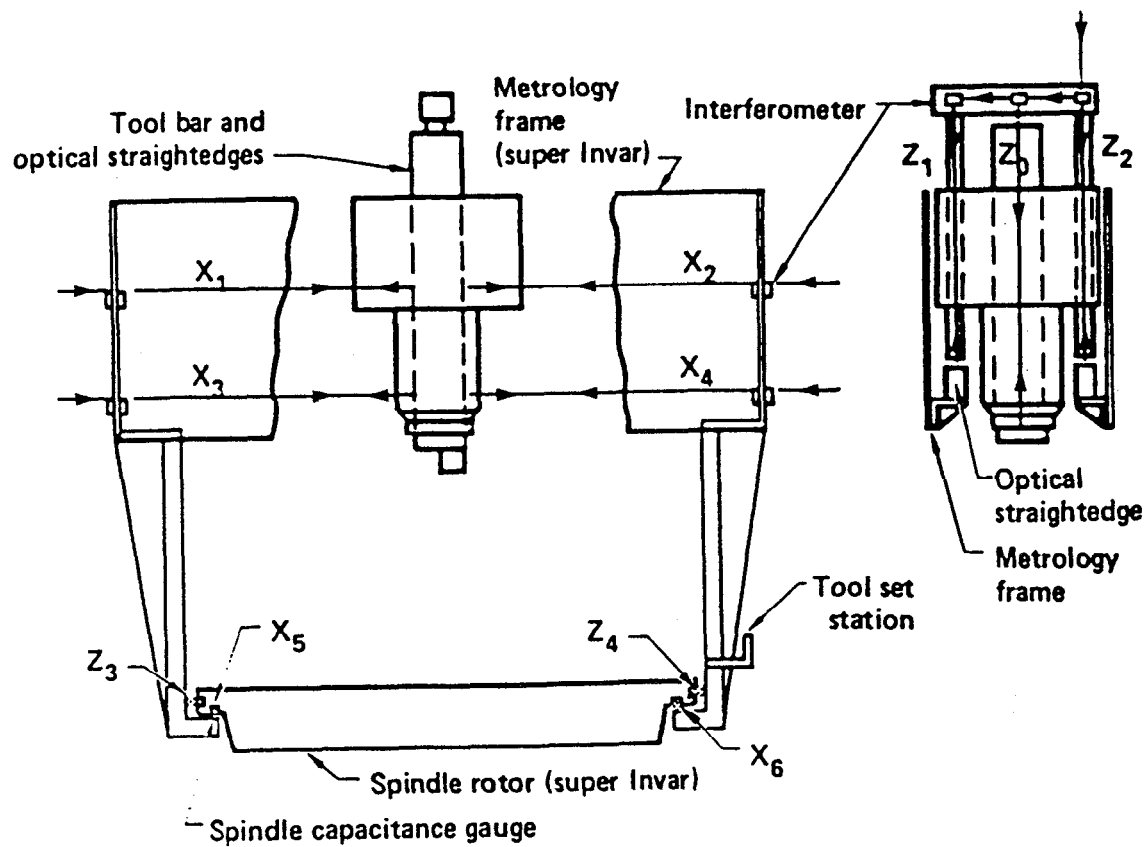
Figure 3.2    Schematic of the LODTM metrology loop.

## 2.  Interferometer System
## 2.1 Optical Heterodyne Interferometry

The fundamentals of ac optical heterodyne detection were developed in the communication field in the I950's and 60's.  Early papers on the method by A. E. Siegman[1] and O. E. DeLange[2] describe the advantages, disadvantages, basic limitations, and potential applications for long distance communication and for detecting Doppler shifts in coherent light scattered by liquids, gases, or small particles.

About this same period dc phase measuring interferometers were being developed for measuring the figure of optical elements, and for alignment purposes.  One of these early instruments is described by Crane[3].

About 1970, the two technologies were successfully combined, and the first optical heterodyne distance measuring interferometers became commercially available[4,5]. The interferometer is usually set up in a Michelson configuration, as shown in Fig. 3. The basic components include:

(1)   a dual-frequency light source with orthogonally polarized collinear beams

(2)   reference and measurement detectors

(3)   a polarizing beamsplitter

(4)   a reference (fixed) reflector

(5)   a movable reflector in the measurement or active arm of the interferometer

The light source emits two orthogonal plane-polarized beams oscillating at frequencies $f_1$ and $f_2$.  A small fraction of each beam is split off near the light source and directed into the reference detector.  The majority of the beam power is directed to a polarizing beamsplitter, which separates the two beams.  The beamsplitter directs the S polarized beam (oscillating at frequency $f_2$) into the reference arm of the interferometer.  The P polarized beam ($f_1$) traverses out and back along the measurement arm of the interferometer, and the two beams recombine at the

Reference
detector

Reference reflector (fixed)

Lens

$f_2$

Polarizing
beamsplitter

Quarter-wave plate

$f_2$

$V_m$

$f_1$

Beamsplitter

$f_1$

Reflector

Dual-frequency
light source

Measurement arm

Quarter-wave plate

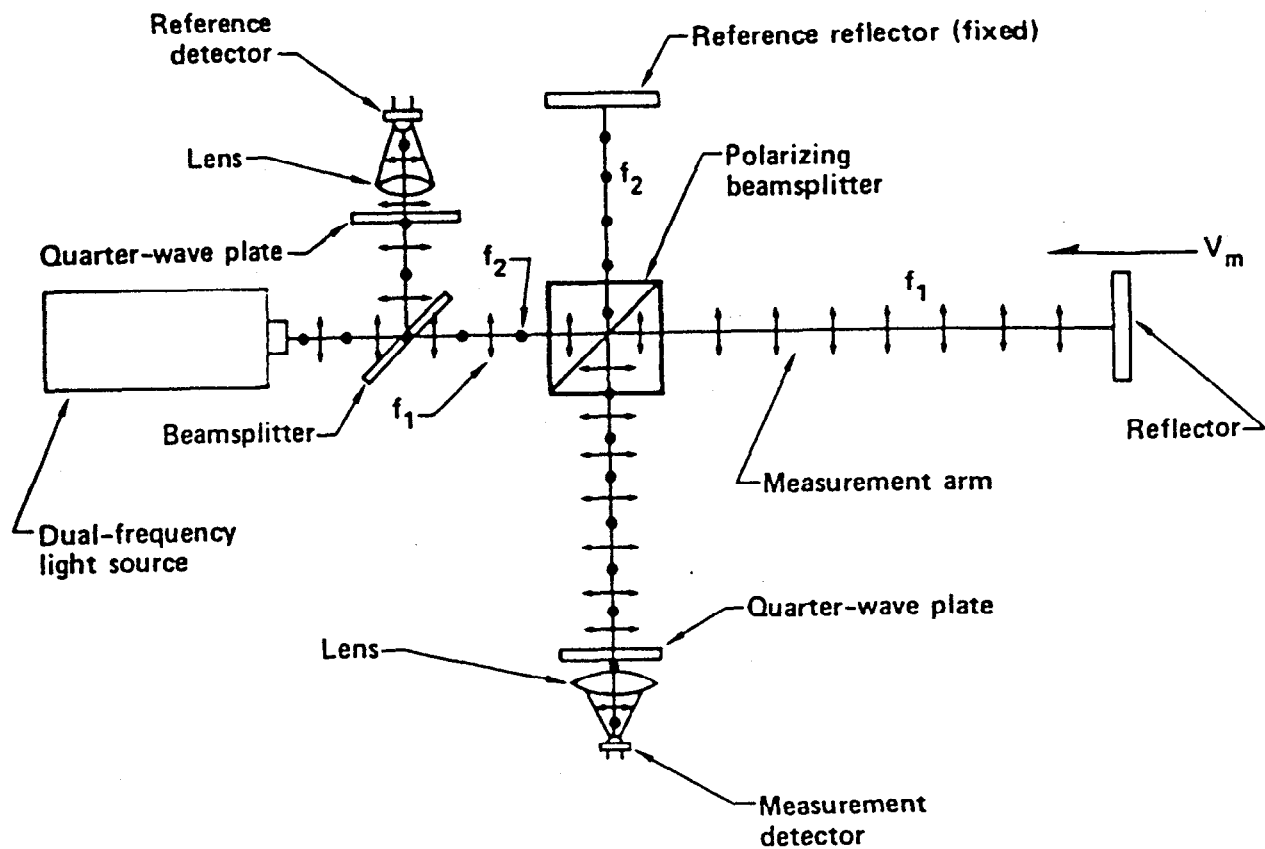Lens

Measurement
detector

Figure 3.3    Beam paths through the optical heterodyne
interferometer.

polarizing beamsplitter surface, from which they then travel collinearly to the measurement detector.

A quarter-wave plate placed in front of the detector with the principle axis oriented at 45° relative to both polarizations, converts the linearly polarized light to right and left circularly polarized light. Interference between the two beams will now occur in a plane parallel to the principle axis of the quarter-wave plate.

Phase detection of the resulting ac measurement signal relative to the reference signal yields an output which is proportional to distance changes in the measurement arm of the interferometer. A derivation of the interference phase relationships is given in Appendix A.

Optical heterodyne interferometry offers some distinct advantages over conventional position transducers such as inductive scales, linear optical encoders, and rotary electrical encoders, that are commonly found on machine tools:

(1) Absolute accuracy in a vacuum is limited only by how accurately the frequency of the light source is known, and the frequency stability of the light source, which can be better than one part in $10^9$, or 1 nm per meter.

(2) Resolution can be made high by refinement of the phase measuring electronics. For LODTM, the value is $\lambda/1024$, or approximately 1/40th of a $\mu$in (0.618 nm).

(3) The system is relatively insensitive to amplitude variations of the light source.

(4) The output signal is easily converted to digital form.

(5) Positional information is available in real time (updated every 1.5 msec for LODTM).

Some disadvantages are:

(1) The system measures relative displacement only -- no absolute information is produced.

(2) Displacement information is lost if either the measurement or the reference beam is optically or electrically interrupted.

(3) A considerable amount of electronic signal conditioning and processing is required.

(4) For beam paths in open air, the measurements must be corrected for the index of refraction, which in turn is a function of pressure, temperature, humidity, and $CO_2$ content. It is difficult to correct the measurements to better than about one part in $10^7$, which is the reason that the LODTM beam paths are enclosed in a vacuum.

(5) To achieve an absolute accuracy of one part in $10^9$, careful attention to a number of design details is required, as discussed in subsequent sections.

The two primary performance requirements for LODTM are:

(1) Surface finish errors [i.e., surface normal errors occurring at spatial wavelengths of 0.004 in (100 μm) or less] shall not exceed 0.17 μin (43 Å) rms.

(2) Radial figure errors (i.e., surface normal errors occurring at spatial wavelengths greater than 0.004 in) shall not exceed 1.1 μin (28 nm) rms over the total machining volume of 64 in (1625 mm) in diameter by 20 in (500 mm) high.

After carefully reviewing the design implications of these two very stringent system performance requirements, and recognizing that only a small fraction of this total error could be allocated to the metrology system, it was concluded that the use of optical heterodyne interferometry offered the highest probability of reaching the above performance goals for the LODTM.

## 2.2 System Performance Requirements

Early in the LODTM Project a detailed analysis was made to identify and evaluate many error sources (see Chap. 3, Ref. 6). Error budgets were then developed using the following method:

(1) Listing the physical effects that can cause errors.

(2) Assessing the magnitude of the resulting machining error.

(3) Assigning the machining errors to the proper workpiece error categories; surface finish, azimuthal figure, radial figure, and slope errors.

(4) Selecting a combinatorial rule for determining the cumulative effect of all machining errors in a given category.

For example, in the error budget for the radial figure, the following error sources were identified and their contributing errors were quantified either by calculation or by an estimate (based on experience with similar systems):

(1) Positional interferometers

(2) Control system

(3) Temperature control

(4) Spindle air supply pressure

(5) Gravitational loading

(6) Barometric pressure

(7) Nonmachine factors, such as:

    (a) Toolnose roundness

(b)  Workpiece fixture distortion

(c)  Workpiece body forces

(d)  Workpiece internal unbalance

(e)  Workpiece residual stress

After the overall machine performance requirements and the error analyses were factored together, the following performance requirements for the LODTM interferometer system were developed:

(1)  Provide a total of seven continuous positional signals in real time (updated every 1.5 ms), four of which are horizontal beams in a fixed X-Z plane (for measuring X displacements), with the three remaining beams being vertical in a Y-Z plane moving with the carriage travel (for measuring Z displacements).

(2)  Positional information shall be resettable to zero in both the X and Z planes, relative to an arbitrary datum (such as the toolset station).

(3)  Least count (resolution) of the interferometer system shall be 0.6l8 nm (0.0243 $\mu$in), i.e., $\lambda$/1024 for the He-Ne wavelength.

(4)  The root sum of the squares of all errors, including those caused by environmental changes, shall not exceed 2.0 nm (0.080 $\mu$in) in 24 hours, for the full carriage travel of 44 in (X direction) and 20 in of toolbar travel (Z direction).

(5)  The long term absolute accuracy of the interferometer least count shall be known and remain constant to within 1 part in $10^9$, indefinitely.

(6)  The interferometer system shall perform as specified in (5) above, while operating within the following environmental conditions:

(a) Ambient air temperature -- 68 ± 0.02 °F

(b) Ambient air humidity -- 20 to 60% RH

(c) Ambient air pressure -- 760 torr ± 10%

(d) Machine temperature -- 68 ± 0.001 °F

(7) The interferometer shall operate within specifications for a continuous period of 10,000 hours without replacement or realignment of major subsystems or components.

## 2.3 Description of Major Subsystems

The interferometer system is composed of five major subsystems:
(1) The light source assembly

(2) The beam modulator assembly

(3) The beam transfer system

(4) The Z-axis interferometer assembly

(5) The X-axis interferometer assembly

These subsystems are schematically shown in Fig. 4 as they are integrated on LODTM.

The light source assembly and beam modulator are mounted on a common base attached to the underside of the LODTM main-frame.

The light source assembly (Fig. 5) consists of a Spectra Physics Model 125A helium-neon laser, an Iodine stabilized helium-neon laser, two laser power supplies, the control system for the Iodine stabilized laser, and laser frequency-lock controls. The

Z
Yaw angle
Y
X
Roll angle
X
Pitch angle
Z
Y

Z-axis optical straightedge (2)

X-axis optical straightedge (2)
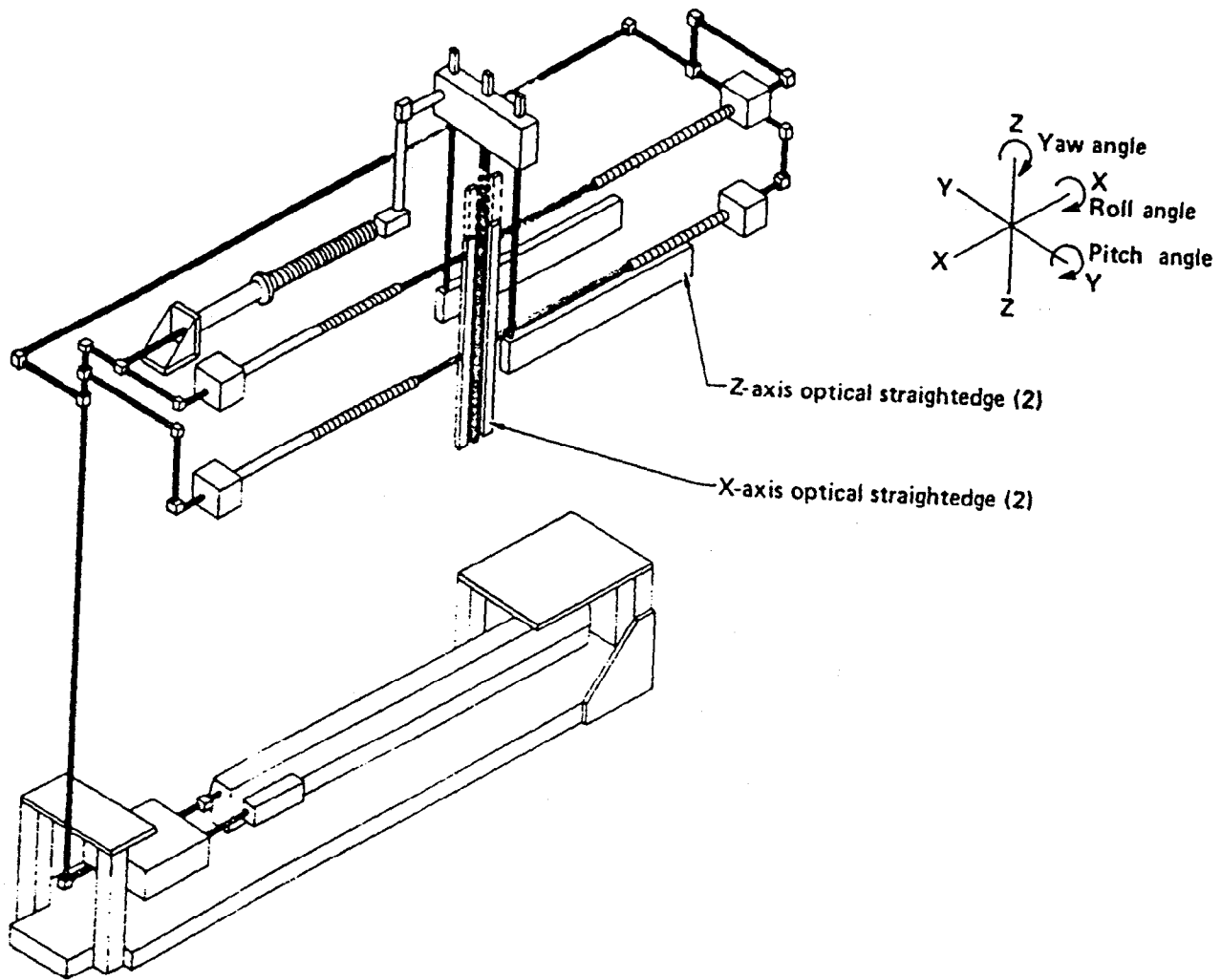
Figure 3.4     General view of the interferometer subsystems.

Plane of polarization
is oriented 45° from
plane of figure

Beamsplitter

Polarization rotator

SP-125A helium-neon laser

To beam
modulator

Beamsplitter

Etalon
control
detector

Iodine stabilized
helium-neon laser

Beamsplitter

Heterodyne
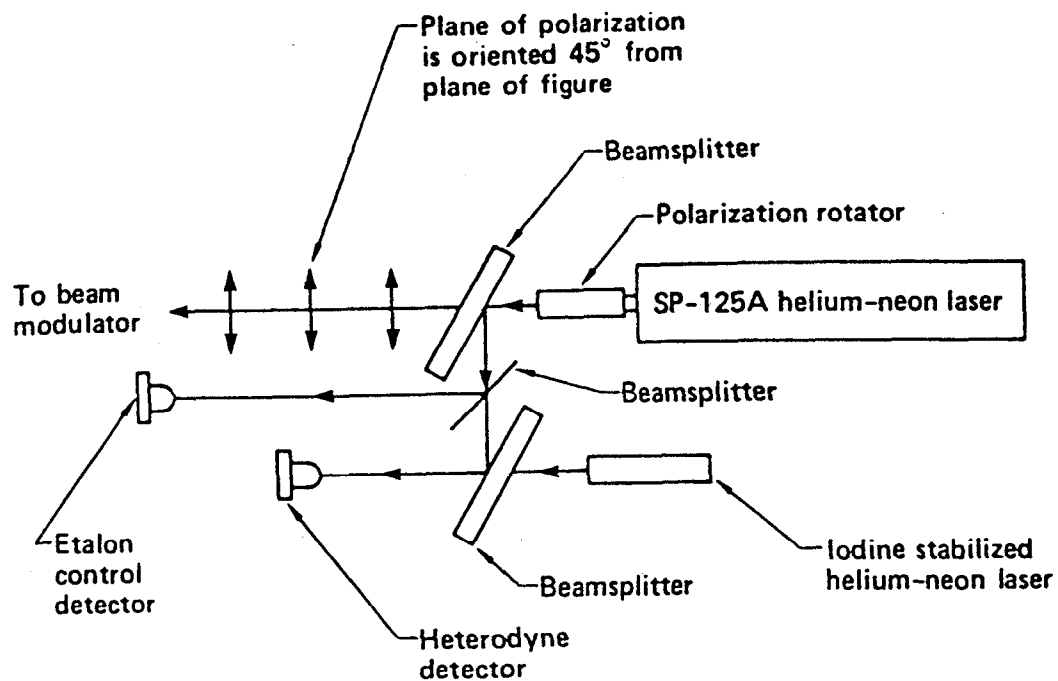detector

Figure 3.5    Schematic view of the light source assembly.

purpose of the light source is to provide a plane-polarized light beam with a cw power output of 10 to 30 mW at a single stabilized frequency and a wavelength of 633 nm.

The beam modulator (Fig. 6) consists of a polarizing beamsplitter, two acousto-optic modulators (Bragg cells), a polarizing beam combiner, and two plane mirrors, arranged as a Mach-Zehnder interferometer. The modulator output is turned 90 degrees by a mirror and directed into a beam expanding telescope with a spatial filter. The modulator takes a single, plane-polarized cw laser beam and converts it into two collinear, orthogonally polarized beams, modulated at 60 and 61.75 MHz (frequency difference of 1.75 MHz). The total power in the expanded output beam is typically 60% of the input.

The beam transfer system consists of a series of mirrors and beamsplitters mounted in adjustable holders and beam enclosures, along with their associated mechanical hardware (Fig. 4). This system takes the single output from the beam modulator, divides it into seven beams of approximately equal intensity, and directs these beams to the seven individual interferometers.

The Z-axis interferometer assembly (Fig. 7) is mounted on the carriage, and consists of three interferometers with their associated beamsplitters, turning mirrors, reflectors, and signal receivers. The center interferometer "looks at" a mirror mounted at the lower center of the hollow toolbar, and measures the vertical (Z-axis) motion of the toolbar relative to the Z interferometer platform. The two outer interferometers each "look at" an aluminized Zerodur straightedge mounted horizontally on the metrology frame on either side of the carriage. The average of the two interferometers measures the relative vertical motion between the Z interferometer platform and the metrology frame at the toolbar centerline. Subtraction of this average from the center interferometer yields the toolbar position relative to the metrology frame.

At each end of the metrology frame (Fig. 2), a pair of X-axis interferometer assemblies (Fig. 8) are mounted in a vertical plane. They "look at" aluminized Zerodur straightedges, one mounted vertically on each side of the toolbar. They measure the horizontal (X-axis) motion of the carriage, plus carriage "pitch", or the angular motion as it moves back and forth along the ways.
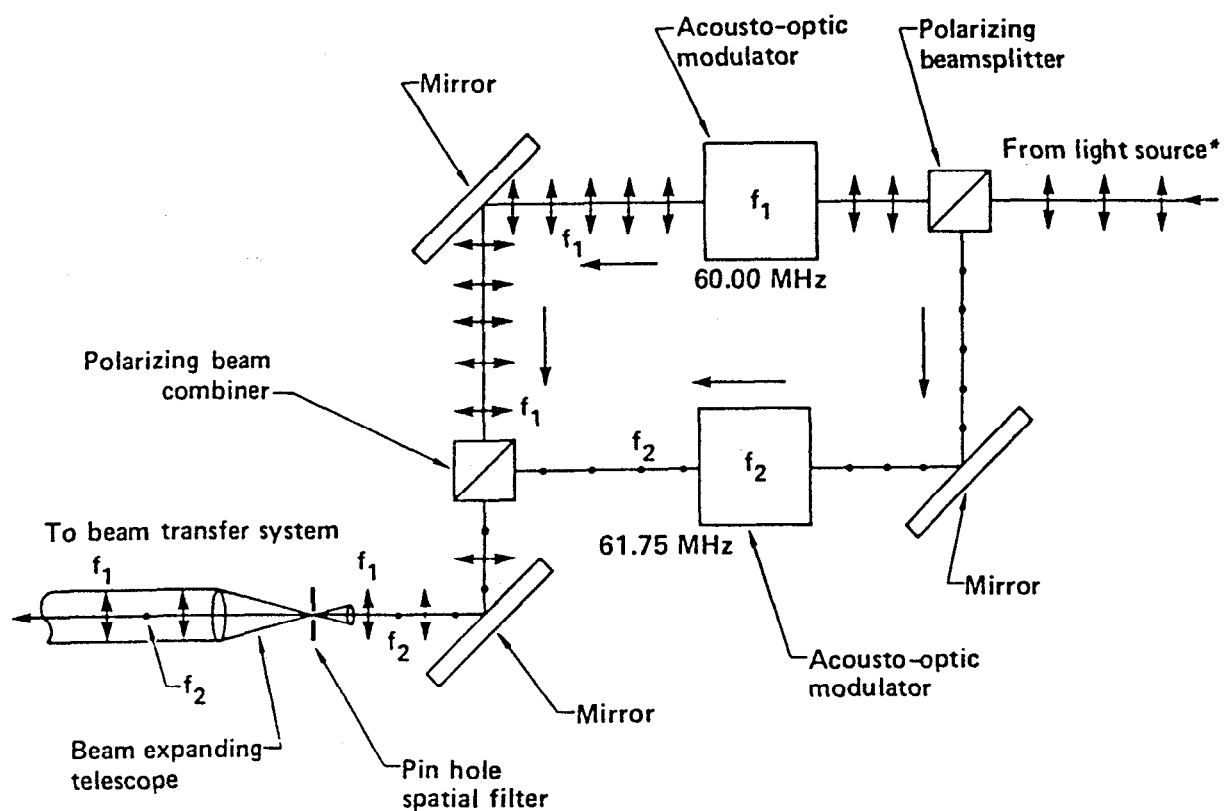
Figure 3.6    Laser beam paths and polarizations in the beam modulator assembly.
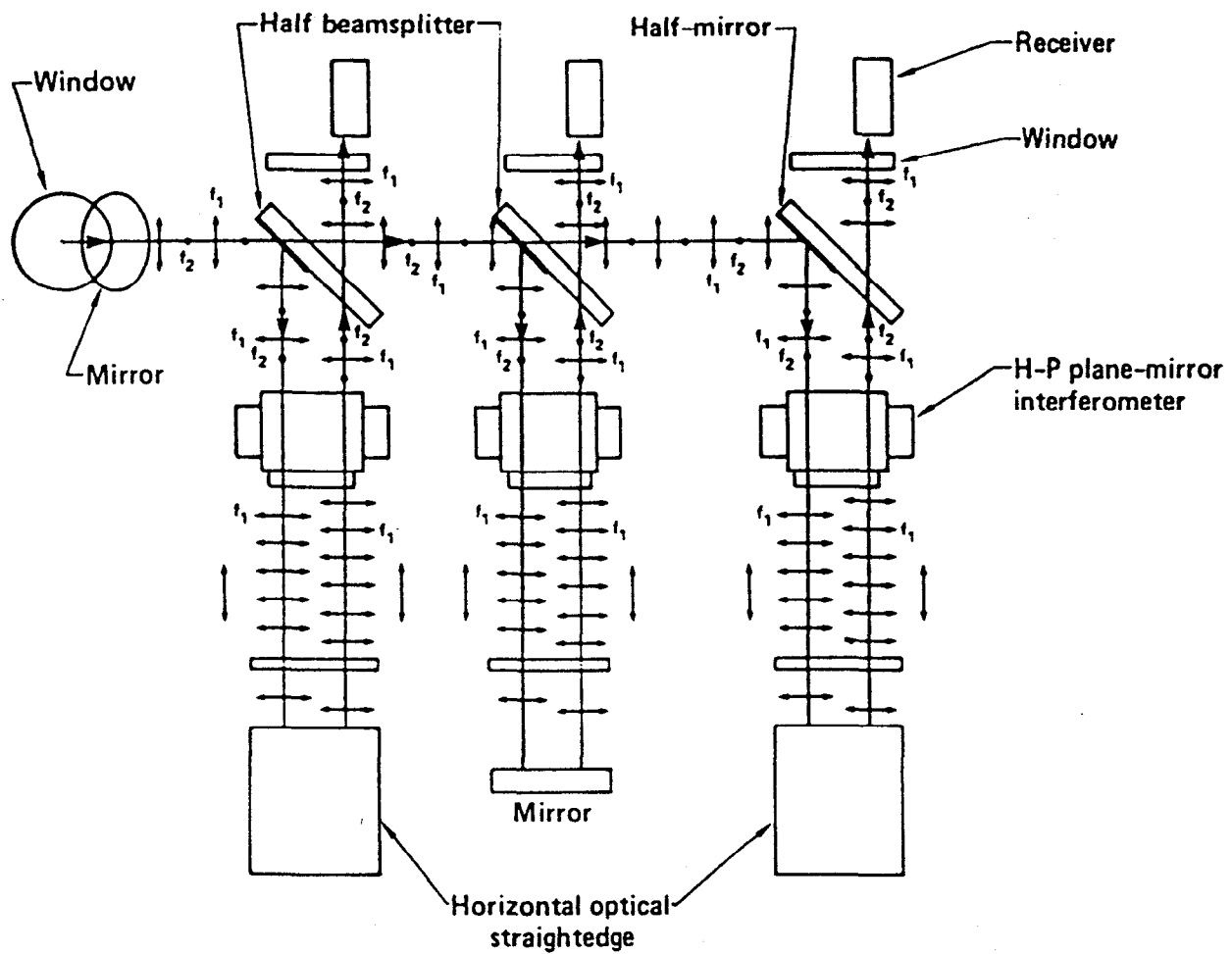
Figure 3.7    Laser beam paths and polarizations in the Z-axis interferometer assembly.

## 2.4 Sources of Error

Optical-heterodyne distance measuring interferometers measure the relative displacement between the reference and measurement arms of the interferometer (see Fig. 3). In the interferometer system for the LODTM (a plane-mirror configuration), the beam traverses the measurement arm four times. A complete light or dark field will then occur in the interference plane (at the detector) according to the equation:

$$m\frac{\lambda}{4} = nD,$$  (1)

where:

$\lambda$  =  the vacuum wavelength of the interferometric light source,

n  =  the refractive index of the medium,

D  =  the length difference between the two arms of the interferometer,

|m|  =  0, 1, 2, -- for a light field, and

|m|  =  1/2, 3/2, 5/2, -- for a dark field.

The optical path difference, nD, between the two arms of the interferometer is more realistically represented by the equation:

$$nD = \Sigma [N_M l_M] \pm \Sigma [N_R l_R],$$  (2)

where:

nD  =  the net optical path difference,

$\Sigma [N_M l_M] =$  the sum of the optical paths of all elements in the measurement arm,

$\Sigma [N_R l_R] =$   the sum of the optical paths of all elements in the reference arm,

l   =   the physical length of an optical element, and

N   =   the index of refraction of an optical element.

Before starting any machining or measuring operation with the LODTM, the cutting edge of the diamond tool is located at a fixed reference point (the tool-set station), and the seven interferometer fringe counters are set to zero. Any uncontrollable change of length in the optical path that occurs after the tool leaves the tool set station, either in the measurement or the reference arm, will produce a displacement error.

Changes in the wavelength of the interferometer light source will also cause similar displacement errors. The third major error source in heterodyne interferometers is caused by phase mixing of the two polarized beams.

Changes in the optical path length of components are minimized in the LODTM by:

(1)   Controlling the temperature of the component by controlling the ambient air temperature to within 0.04 °F peak-to-valley (P-V),

(2)   Minimizing the air path length in the measurement arm through the use of evacuated bellows and beam tubes, and

(3)   Where air paths exist (between windows and straightedges), minimizing differences in temperature, pressure and gap length between the air paths, so that cancellation of equal effects can occur.

To calculate the amount of change in the optical path difference (OPD), in a component that is being caused by temperature changes, the changes in both physical length and refractive index must be accounted for. The overall change for a single pass through a refractive component can be calculated from the equation:

$$OPD = L\left[\alpha(n-1) + \frac{dn}{dt}\right]\Delta t \qquad (3)$$

where;

$$L = \text{the length of the component,}$$
$$a = \text{the coefficient of linear expansion,}$$
$$n = \text{the refractive index relative to vacuum, and,}$$
$$\Delta t = \text{the component temperature change.}$$

For example, windows in the interferometric measurement arms are 0.4 in thick and are made from the best quality Schott BK-7 glass. The interferometer beam passes through them four times. A temperature change of 0.04 °F P-V will result in an OPD of 0.15 μin P-V, with an RMS variation of 0.044 μin, using:

$$RMS = \frac{1}{2\sqrt{3}} \sum_{i=1}^{N} (P - V)^{2^{1/2}} \qquad (4)$$

(see Sec. 1.8, Ref. 6).

The major factor limiting high-accuracy displacement measurements in air is uncertainty in the absolute value and temporal variations of the refractive index of air. Variations in the refractive index of air are caused by changes in its temperature, pressure, and relative humidity. Under the best conditions of measurement and compensation, the uncertainty in the displacement measurement would be about ± 5 parts in $10^8$ (Ref. 7). This does not meet the LODTM interferometer requirement that the root sum of the squares (RSS) of all measurement errors along a single axis of movement should not exceed 2 parts in $10^9$ (0.08 μinches in 44 inches of X-axis travel).

For this reason we designed the LODTM interferometers to operate in a partial vacuum, with an air pressure of about $14 \pm 1$ millitorr or less over the entire length of the measurement arm, except for a small air gap (0.030 ±.001 in) between the interferometer window and the aluminized optical straightedge.

The interferometers in the X- and Z-axis systems are configured to operate differentially. For the X-axis system, two pairs of interferometers are arranged in a vertical plane, so that the top pair and the bottom pair each "looks" at collinear points on a horizontal line, on opposite sides of the toolbar. Thus, for a horizontal pair, a plus

X-axis displacement on one interferometer is measured as the exact minus X-axis displacement on the opposing interferometer.

Refractive index variations in the air gaps between the interferometer windows and the reflective straightedges can result in two types of errors: one caused by local pressure differences between opposite gaps, and one caused by the tolerance on the length of opposed air gaps. Typical errors of this type are 0.013 $\mu$in and 0.032 $\mu$in, respectively. (See Table 1, Error Summary for a Single LODTM Interferometer).

Section 2.1 explains how an optical heterodyne interferometer operates. Displacement changes in the measurement arm are determined by detecting the relative phase shift between the reference and measurement arm beams.

If part of the measurement beam (frequency $f_1$ in Fig. 3) "leaks" into the reference arm (or vice versa), a phase error will be generated at the detector. A mathematical description of this error is given in Appendix A. The error is periodic, and passes through a maximum or minimum every 180° of phase shift between the two beams. The magnitude of the error is a function of the amplitude of the undesired signal (of opposite polarization) that enters each arm of the interferometer.

Undesired beam (polarization) mixing in the two arms can be caused by:

(1) Non-orthogonality between the two planes of polarization at the entrance of the interferometer.

(2) Angular misalignments between the planes of polarization and the separation plane of the polarizing beamsplitter.

(3) Separation limitations of the polarizing beamsplitter coating.

(4) Phase shift properties of corner reflectors. One corner reflector is used in each arm of the plane-mirror interferometer (see Appendix A, Fig. A-1).

(5) Birefringence in optical elements, which include the polarizing beamsplitter, corner reflectors, and windows.

The polarization mixing properties of the beamsplitters and corner reflectors were measured, and the effects of birefringence in glass and fused silica were calculated from data supplied by the manufacturer. Misalignment effects were calculated from estimates of alignment errors.

The combined effects of all polarization mixing factors gave a calculated beam-mixing intensity of 0.08%. This intensity amplitude was used in equations 16 and 18 of Appendix A to calculate the resultant maximum phase error, $\theta$. For the LODTM plane-mirror interferometer, this phase error (about 6.5°) would produce a maximum periodic (P-V) error of 0.112 $\mu$in, or an RMS error of 0.032 $\mu$in.

The complete error budget for a single LODTM interferometer is summarized in Table 1. The total root-sum-of-the-squares (RSS) for all the errors is 0.08 min. This includes periodic errors (Item 1), short term varying errors (Item 2), longer term varying errors caused by changes in atmospheric pressure (Item 3), and errors caused by changes in component temperatures (Items 4-6).

## 2.5 Design and Fabrication of Optical Components
### 2.5.1 General Requirements

In optical-heterodyne-detection, the signal current is directly proportional to the power. It will be maximized if the optical phase is uniform over the complete wavefront of both coincident beams at the plane of interference (plane of detector). According to DeLange[2], obtaining a uniform optical phase requires that:

(1) The beams must have the same transverse mode structure.

(2) The beams must be colinear, and to provide the maximum signal-to-noise ratio, their diameters must be equal.

(3) The beams must propagate in the same direction; that is, their Poynting vectors must be coincident.

(4) The wavefronts must have the same curvature.

(5)  The beams must be identically polarized, so that their electric vectors will be coincident.

In the LODTM interferometer system, some beam paths from the laser to the receiver are as long as 47 ft (14 m), and the reference and measurement beam paths are unequal by as much as 33 ft (10 m), depending on the position of the carriage or toolbar. A typical measurement-arm beam traveling from the laser to an interferometer receiver will pass through 15 in (0.4 m) of glass and fused silica, 64 optical surfaces, and will experience 21 reflections from beam transfer and retroreflector components.

About 2 mW of single-mode beam power is available at the beam modulator exit for each of the seven interferometers (a total of 14 mW for both polarized beams). It is desired to have from 140 to 200 μW of beam power (from 7% to 10% of the available power) incident on each interferometer.

The requirements for uniform optical phase, minimum beam-power loss, and low polarization-mixing (0.08% intensity) errors, placed stringent requirements on the quality and performance of most optical components and coatings. The design, fabrication, and quality control of these components are described in the next subsection.

### 2.5.2  Interferometer Components

Hewlett Packard (H-P) plane-mirror interferometer components were selected for use on the LODTM because:

(1)  They are designed for use with Helium Neon lasers.

(2)  Their optical performance meets the stringent LODTM requirements for low levels of polarization mixing.

(3)  They are designed to operate in a vacuum.

(4)  Their mechanical mountings are designed for long-term angular stability in the μradian range.

## Table 1

### Error Summary for a Single LODTM Interferometer.

| Error Source | Estimated RMS[a] Error ($\mu$in) |
|---|---|
| (1)  Polarization mixing (0.08% intensity) | 0.032 |
| (2)  Air gap pressure variation<br>(0.030 in gap, $\Delta P = 1$ torr, 4 passes) | 0.013 |
| (3)  Air gap setting uncertainty<br><br>($\Delta$ gap = 0.001 in, $\Delta P = 76$ torr, 4 passes) | 0.032 |
| (4)  Change in window temperature<br>($l_w = 0.4$ in, $\Delta t = 0.04$ °F, BK-7 glass, 4 passes) | 0.044 |
| (5)  Change in interferometer temperature<br>($l_i = 1$ in, $\Delta t = 0.02$ °F, BK-7 glass, 2 passes) | 0.028 |
| (6)  Change in quarter-wave-plate temperature<br>($l_{QWP} = 0.2$ in, $\Delta t = 0.02$ °F, quartz crystal, 4 passes) | 0.039 |
| | RSS = 0.080 $\mu$in[b] |

$$^a RMS = \frac{1}{2\sqrt{3}} \left[ \sum_{i=1}^{N} (P - V)^2 \right]^{1/2}$$

$$^b RSS = \left[ \sum_{i=1}^{N} (RMS)_i^2 \right]^{1/2}$$

## Table 1

### Error Summary for a Single LODTM Interferometer.

| Error Source | Estimated RMS[a] Error (µin) |
|---|---|
| (1) Polarization mixing (0.08% intensity) | 0.032 |
| (2) Air gap pressure variation<br>(0.030 in gap, $\Delta P$ = 1 torr, 4 passes) | 0.013 |
| (3) Air gap setting uncertainty<br><br>($\Delta$ gap = 0.001 in, $\Delta P$ = 76 torr, 4 passes) | 0.032 |
| (4) Change in window temperature<br>($l_w$ = 0.4 in, $\Delta t$ = 0.04 °F, BK-7 glass, 4 passes) | 0.044 |
| (5) Change in interferometer temperature<br>($l_i$ = 1 in, $\Delta t$ = 0.02 °F, BK-7 glass, 2 passes) | 0.028 |
| (6) Change in quarter-wave-plate temperature<br>($l_{QWP}$ = 0.2 in, $\Delta t$ = 0.02 °F, quartz crystal, 4 passes) | 0.039 |
| | RSS = 0.080 µin[b] |

$$^a RMS = \frac{1}{2\sqrt{3}}\left[\sum_{i=1}^{N}(P - V)^2\right]^{1/2}$$

$$^b RSS = \left[\sum_{i=1}^{N}(RMS)_i^2\right]^{1/2}$$

Edited by hand
(columns, square
brackets) - not
in word processor

Figure 9a shows an assembled H-P plane-mirror interferometer, consisting of a polarizing beamsplitter, two corner reflectors, and a quarter-wave plate. A schematic of the interferometer with its plane reflector is shown in Fig. 9b. Since the coated polarizing-beamsplitter cube is mounted inside the case, it is not visible in Fig. 9a.

We measured the polarization mixing properties of several H-P polarizing beamsplitters. With optimum alignment, the components of S and P polarizations that were reflected and transmitted into the wrong arm of the interferometer were about 0.005% of the original beam intensity. This is a small amount compared to the total polarization-mixing error budget of 0.08%. The beamsplitter coatings were also found to be relatively insensitive to small angular misalignments in pitch and yaw. In our error budget, allowable angular misalignments were $\pm$ 1°, $\pm$ 1/4°, and $\pm$ 11' in yaw, pitch, and roll angles, respectively.

The silvered corner reflectors were found to exhibit some unexpected polarization mixing properties, depending upon the relative orientation of the entrance beam and the intersection of the reflecting planes. Experimental results of this mixing relationship are shown in Fig. 10. A photograph of a mounted H-P corner reflector is shown in Fig. 12.

If an incident beam $E_p$, which is polarized perpendicularly to the plane of Fig. 10, is rotated clockwise around the face of the corner reflector, some of the exit beam, $R_s$, will be polarized parallel to that same plane. Since our interferometer beam subtends about 60° of the corner reflector (see Fig. 11), a minimum of polarization mixing occurs when the center of the incident beam is located at 30°, 150°, and 270° (see Fig. 10). At positions of 90°, 210°, and 330°, the polarization mixing has an intensity in the range of from 0.04 to 0.045%. Since this would be the major part of our total polarization mixing error budget of 0.08%, all LODTM interferometers were assembled to locate the entrance beam as shown in Fig. 11. At this location, the mixing was so low it was not measurable.
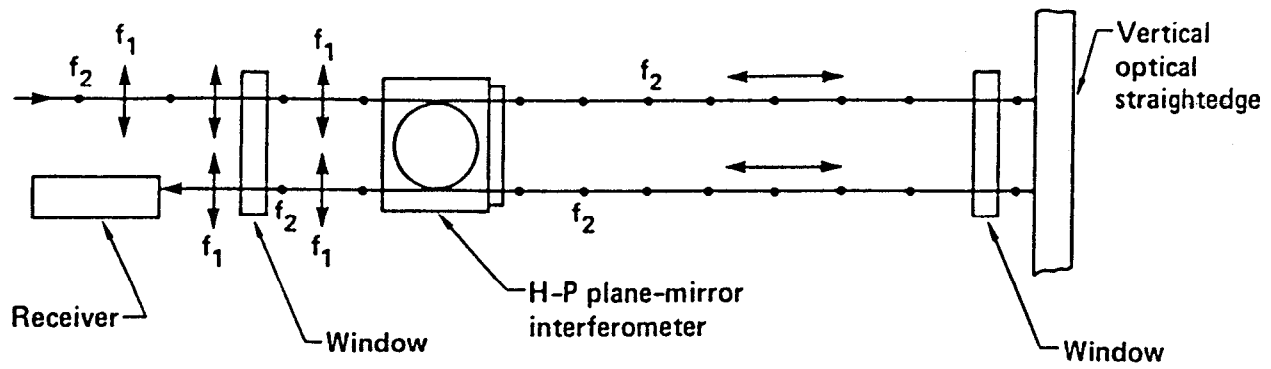
Figure 3.8    Laser beam paths and polarizations in an X-axis interferometer assembly.
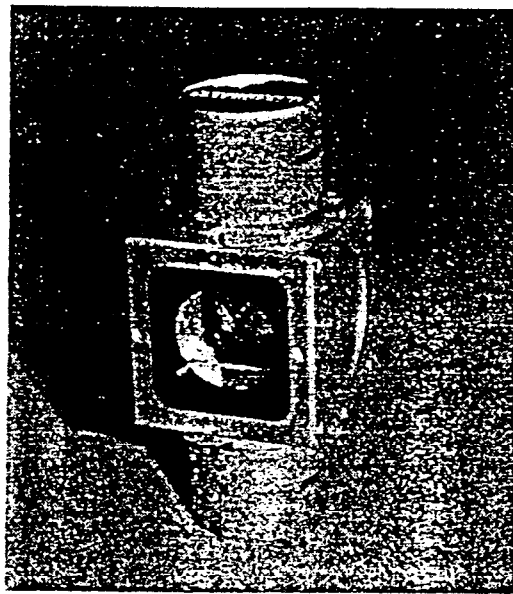


Figure 3.9a    Photograph of an assembled H-P plane-mirror interferometer.
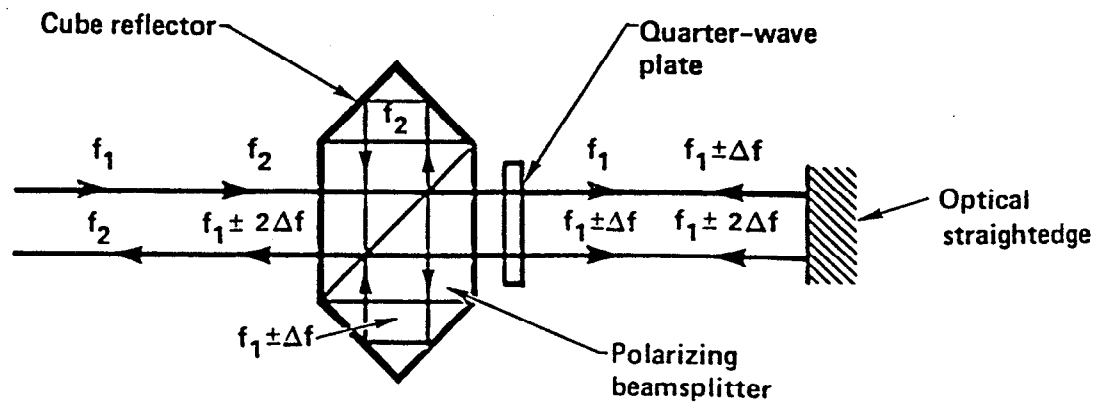


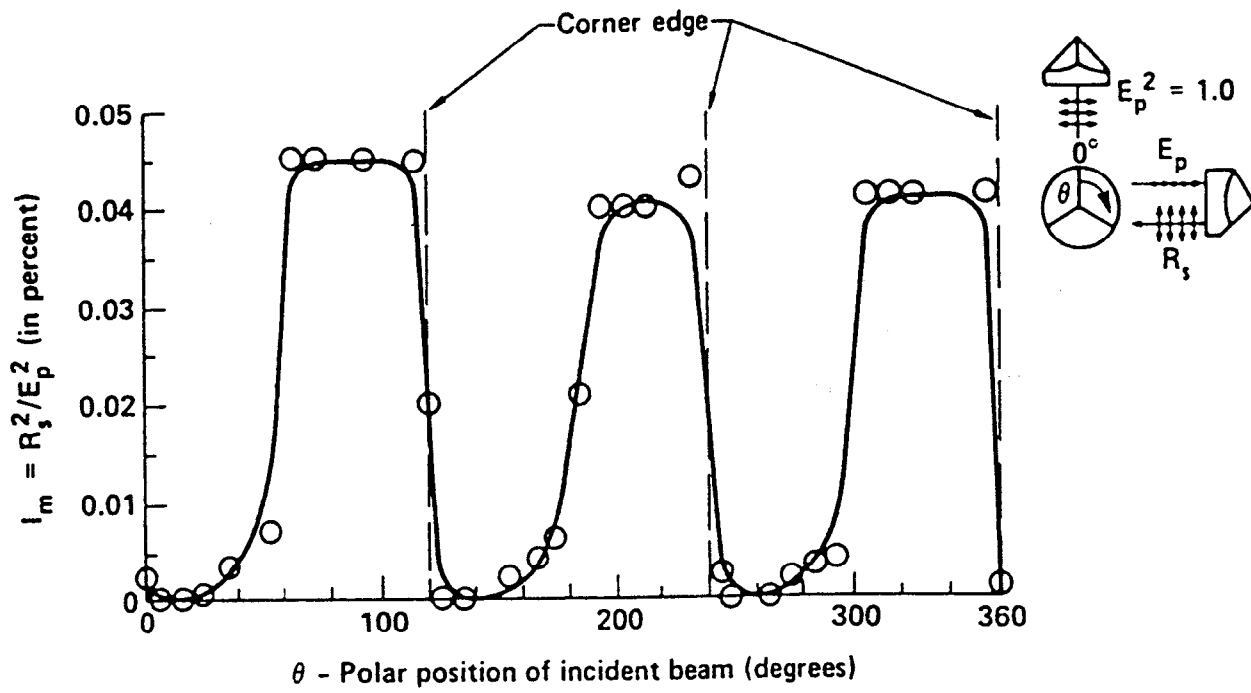Figure 3.9b    Laser beam path through a plane-mirror interferometer.

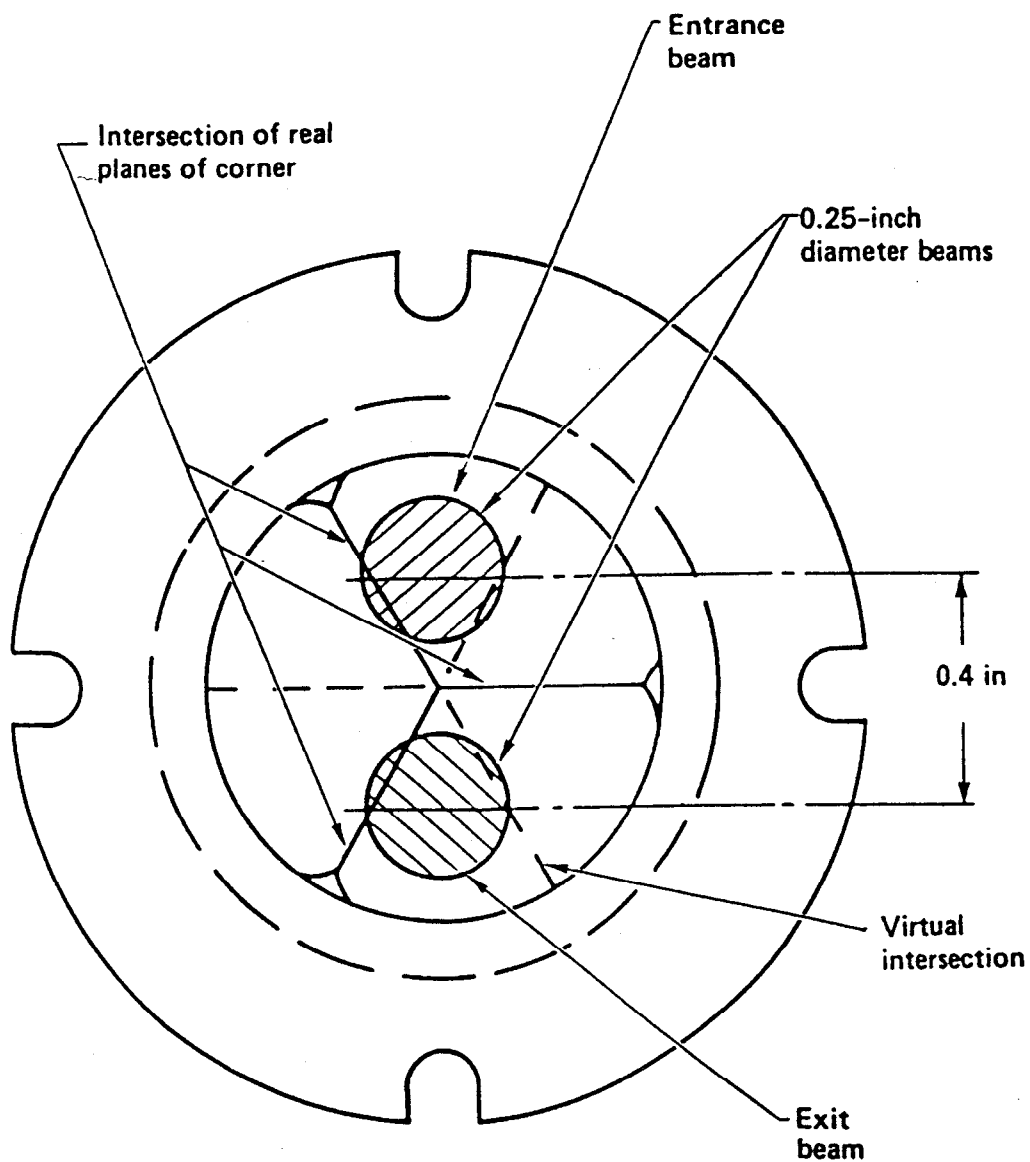Figure 3.10    Polarization mixing characteristics of a silvered corner reflector.

Figure 3.11    Hewlett-Packard corner reflector 10703A, viewed from the flat side.  The beam orientation shown yields the minimum amount of X-axis interferometer polarization mixing.

Figure 3.12     A mounted H-P corner reflector.

## 2.5.3  Window and Beamsplitter Substrates

(See Drawings AAA 81-103516 and 81-103515).  The substrate material for windows and beamsplitters was selected for low residual stress birefringence and good refractive index homogeneity.  Schott BK-7, PH-3 quality glass was used throughout.  The specified refractive index homogeneity was $2 \times 10^{-6}$ or better over any 30 mm diameter of blank, and the maximum residual strain birefringence was not to exceed 6 nm/cm.

It was specified that the single-pass wavefront distortion was not to exceed 1/10 wave at $\lambda$ = 633 nm.  All windows and substrates were interferometrically tested to assure that this requirement was met.

## 2.5.4  Mirrors

(See Drawing AAA 81-103517).  Mirror substrates were made from optical grade B, clear fused silica.  Both flat sides were polished to avoid creep-type warping.  Reflective sides were finished flat to 1/20 wave for $\lambda$ = 633 nm, coated with vapor deposited aluminum, and overcoated with silicon dioxide.  All finished mirrors were interferometrically tested for flatness.

## 2.5.5  Straightedges

(See Drawings AAA 81-103477 and 81-103580).  The plane mirror for six of the seven interferometers is a polished, coated, Zerodur straightedge.  Reflective surfaces are coated with vapor deposited aluminum and overcoated with silicon monoxide.  Two horizontal straightedges are mounted on the metrology frame and are the mirrors for the two outside Z-axis interferometers (see Fig. 4).  One vertical straightedge is mounted on each side of the toolbar and serves as a reflector for two each of the X-axis interferometers (Fig. 4).  These straightedges are among the most important parts of the interferometer system, and they presented some unusual challenges in fabrication, calibration, and design of mountings.

The vertical (X-axis) straightedges are shown in Fig. 13.  All straightedges were made from Schott Zerodur, special grade, selected for low striae and inclusion content, and
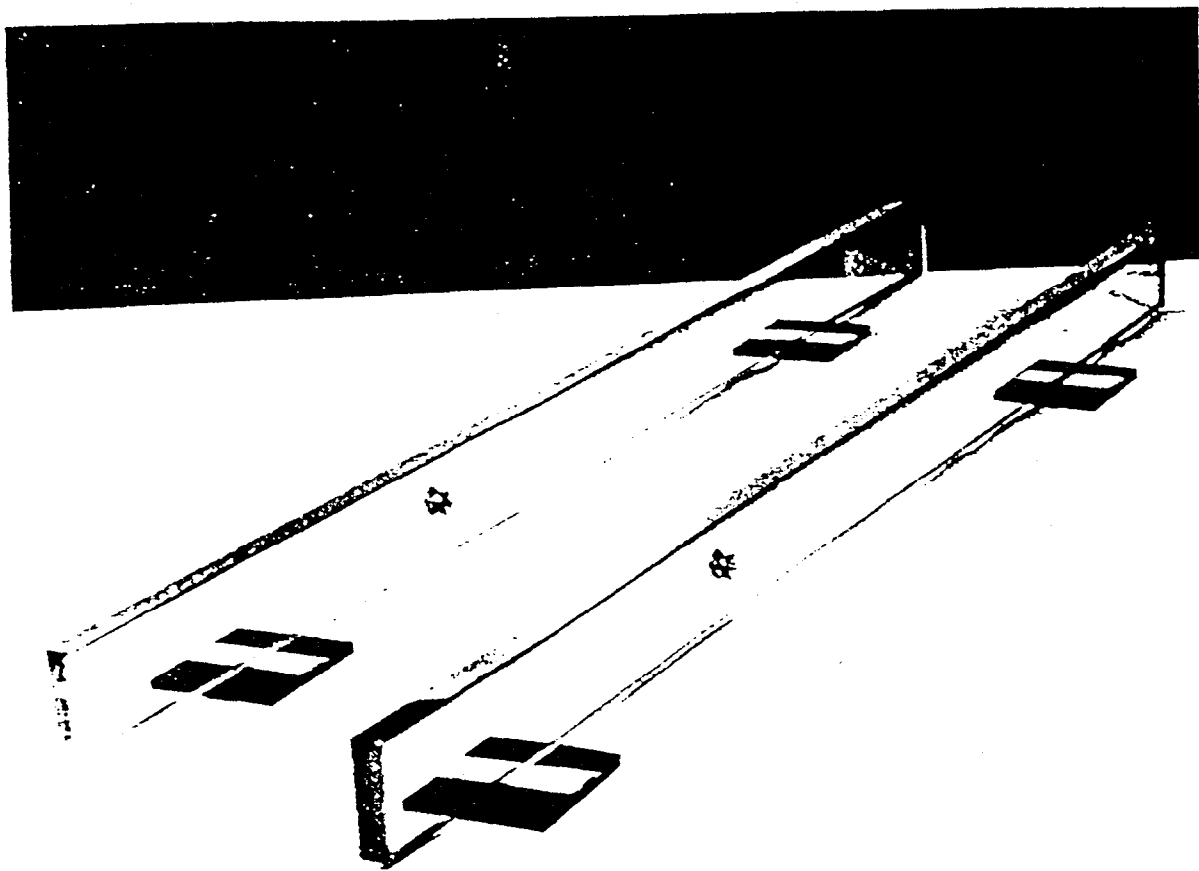
Figure 3.13   The Zerodur vertical optical straightedges used in LODTM.

low stress birefringence. All surfaces were finished by polishing to avoid creep-type warping.

The reflective surfaces were finished on a 144 in diameter continuous-polish (CP) pitch lap. The final surface figure of seven straightedges (3 spares) was tested interferometrically, and all surfaces were found to be flat to within 1/2 wave for $\lambda = 633$ nm. This was a noteworthy achievement for the fabricator, considering the adverse aspect ratio of the straightedge shapes. The width-to-length ratio was 1:57 for the vertical (X-axis) straightedges.

The figure error of one spare horizontal (Z-axis) straightedge was measured by the National Bureau of Standards (NBS) on a special coordinate measuring machine[8]. The results of their measurements are shown in Fig. 14. The reflective surface was found to be concave with a maximum depression of 12 $\mu$in. This spare straightedge was later probed while placed on the LODTM spindle, and knowledge of its figure error was used to correct the straightness error of the X axis in the Z direction, by loading a look-up table in the control computer.

The vertical straightedges were kinematically mounted to the toolbar on flexure-spring mounts, which were carefully designed to isolate the straightedges from loads caused by small deflections of the toolbar. The upper and lower mounts of a vertical straightedge are shown in Fig. 15. The horizontal straightedges are mounted to the metrology frame on a vee, cone and flat, with pitch and roll adjustments provided.

### 2.5.6 Coatings

Anti-reflection (AR) coatings were made from vacuum deposited thin layers of hard dielectrics by alternating layers of ($T_1O_2/S_1O_2$), and the transmittance per surface was typically 0.997 (or higher) at normal incidence for the design wavelength of 633 nm. This is fairly standard performance for modern narrow-band AR coatings.

Beamsplitter coatings for the beam transfer system presented some challenges in their design and deposition. These coatings were designed to have equal reflectance and transmittance for both the S and P polarizations at an angle of incidence of 45°. In most multi-layer designs, the reflectance curves for the S and P components will converge and diverge as a function of wavelength. The goal was to produce a coating
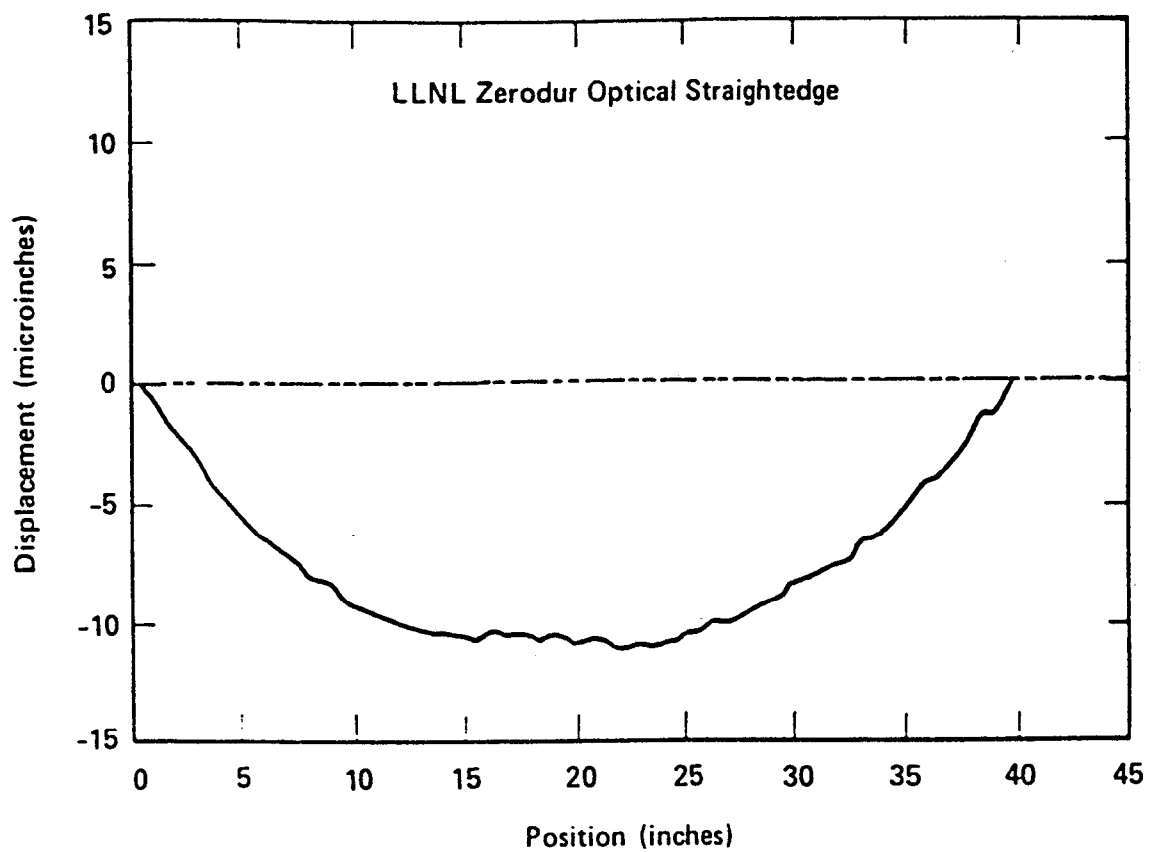
Figure 3.14   The NBS figure error test results for a 40 inch section of the Zerodur horizontal optical straightedge.
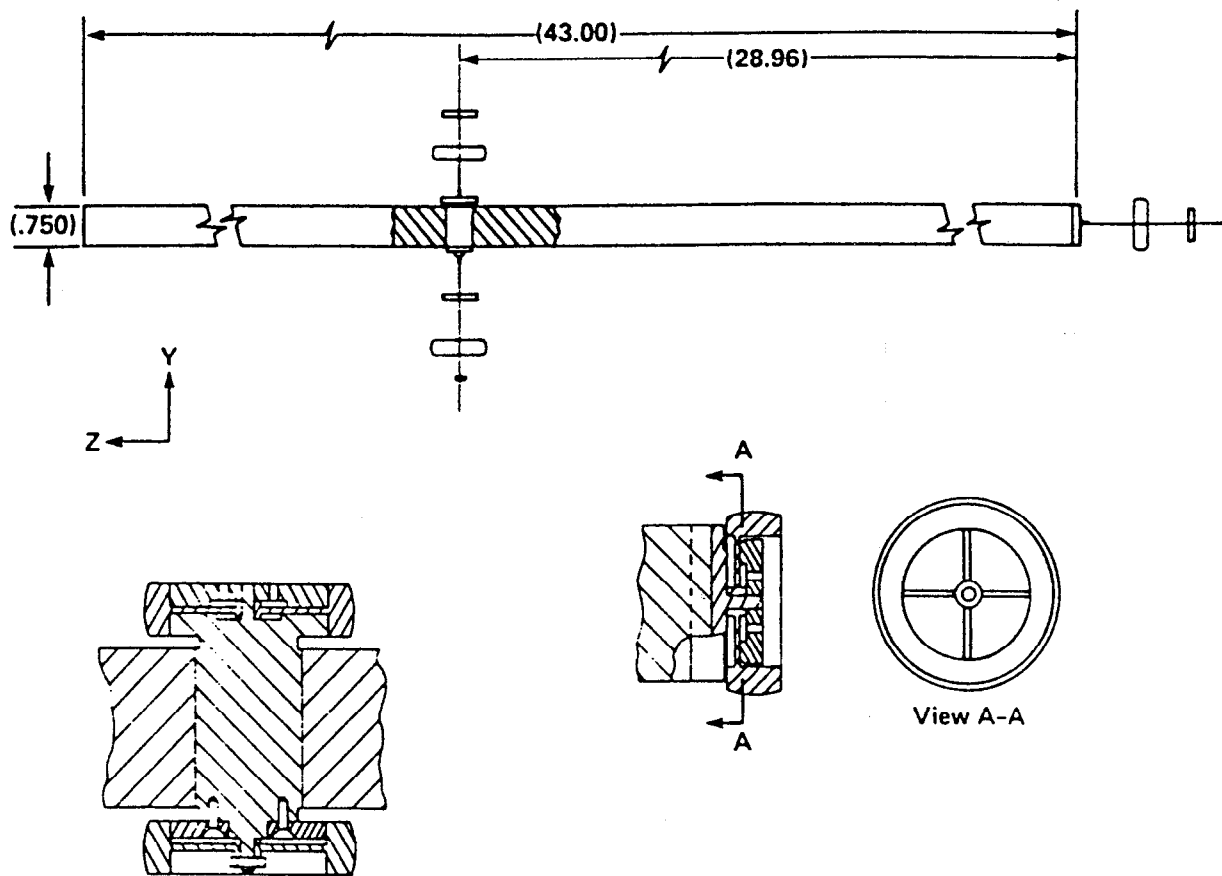
Figure 3.15 Sectional views of the upper and lower mounts for the vertical optical straightedges.

where the difference in reflectivity of the two components at the design wavelength (633 nm for the LODTM system) is within acceptable limits. Figures 16 and 17 show the measured reflectance vs wavelength curves for two typical LODTM beamsplitters. The coating in Fig. 16 was designed to reflect 30% of both components at 633 nm. The measured curves cross at 26% R, an acceptable 4% below the design goal of 30%. In Fig. 17 both the components ($R_S$ and $R_p$) are within ± 5% of the nominal design reflectance of 90%.

## 2.6    Design of Mechanical Components

### 2.6.1    General Requirements

The mechanical components were designed to:

(1)    Provide physically stable platforms or mounting surfaces for optical subassemblies.

(2)    Provide a means for adjusting linear and angular displacement of optical components.

(3)    Maintain constant angular and positional alignment of interferometer beams over year-long times. Interferometer beams must be aligned and remain normal to the moving reflectors within ± 7 sec of arc. The X-Y position of the focused beam at the beam modulator spatial filter must not vary more than 100 µin.

(4)    Protect optical components from external contamination.

(5)    Provide a vacuum environment for all seven interferometers with a constant pressure of 14 ± 1 millitorr.

(6)    Provide a means of repeatably positioning major subassemblies for reinstallation after removal from LODTM for maintenance.

Type 300 stainless steels were generally used for all vacuum enclosures and turning mirror sub-bases. These parts were hot vapor-degreased before assembly.
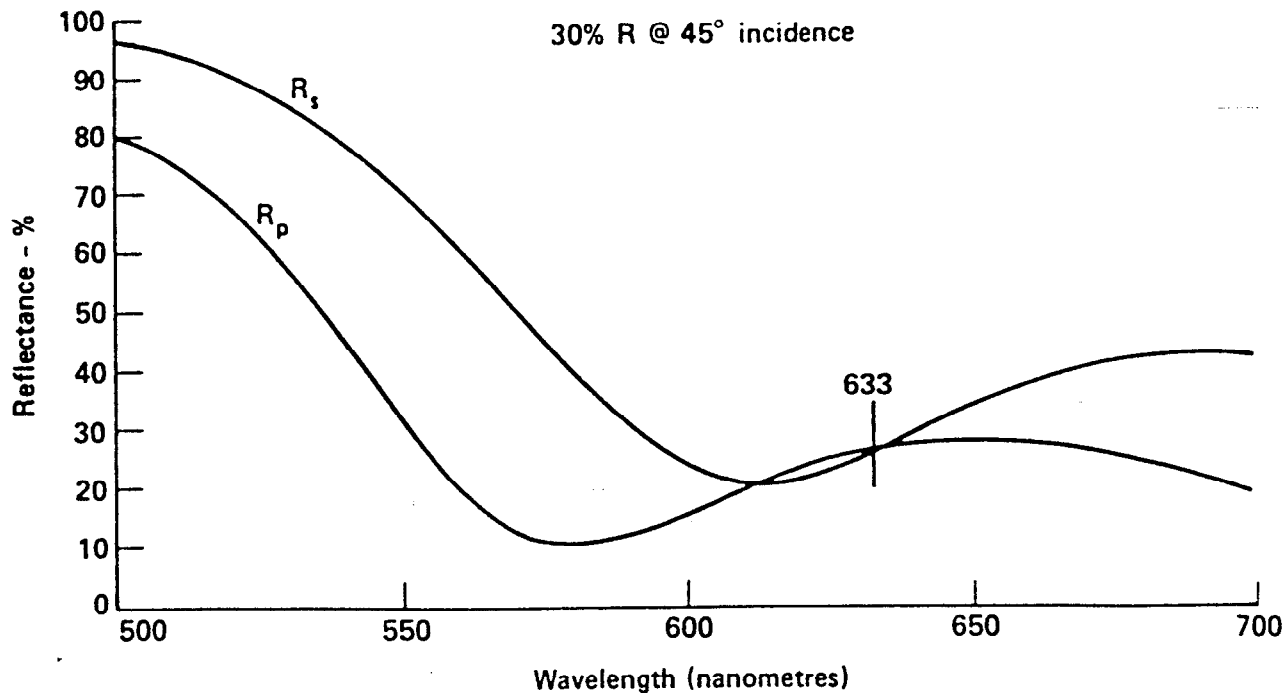
30% R @ 45° incidence

Figure 3.16 The measured reflectance of a beamsplitter designed for 30% reflectance at 633 nm.
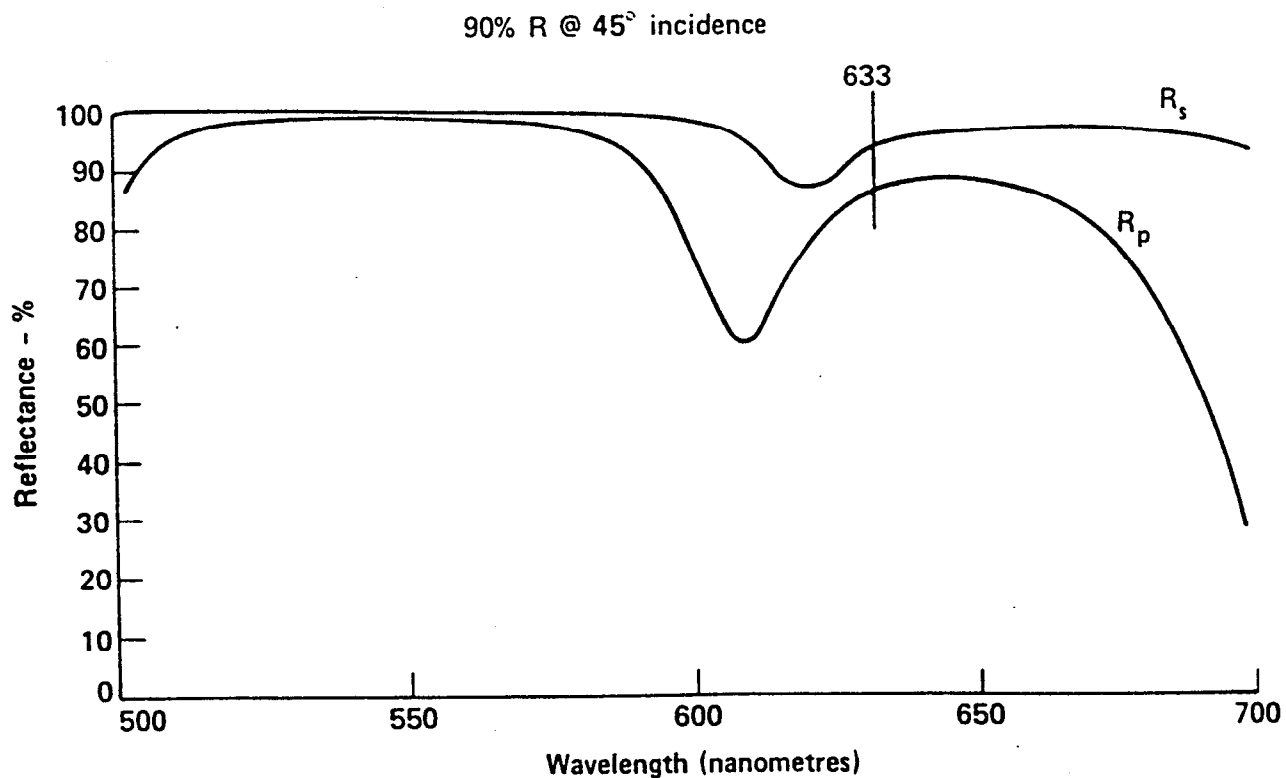


90% R @ 45° incidence

Figure 3.17 The measured reflectance of a beamsplitter designed for 90% reflectance at 633 nm.

Low-expansion material (superinvar) was used for mounting interferometer parts to minimize alignment changes caused by thermal effects. Solid flexure pivots were extensively used in the adjustable mountings for the reflective straightedges, turning mirrors, and the Z-axis interferometer frame. Three-point kinematic mounting was used for the Spectra Physics 125 Helium Neon laser, the Iodine-Stabilized He-Ne laser, and the Z-axis interferometer frame.

Finite-element stress/deflection analyses were used to help design the subsystem platforms and mountings, covers, and structural supports, to assure that the natural frequency of these components was 130 Hz or higher, to minimize vibration and acoustical coupling effects on critical optical components.

## 2.6.2  X-axis Interferometer

(See Assembly Drawing 81-103518). Details of the X-axis interferometer assembly are shown in Figs. 18 to 21. Figure 18 is a view of a partially assembled unit. A H-P plane-mirror interferometer is shown in the lower left corner, along with its superinvar box-type mounting. This mounting is supported on each end by a 0.75 in diameter shaft which protrudes through the side of the vacuum enclosure (see Fig. 20). The outer end of each shaft is attached to the metrology frame when the interferometer is mounted on the LODTM, while the vacuum enclosure is attached to the LODTM mainframe.

A vacuum seal around the shaft is provided by a specially molded "door-knob" boot of polyurethane, selected for its flexibility and low out-gassing properties. Its purpose is to maintain vacuum while avoiding mechanical loading of the interferometer mount and metrology frame due to small thermal or mechanical size and shape changes of the mainframe.

The interferometer measurement-arm beams are enclosed in a stainless steel bellows (not shown in Figs. 18 to 21). One end of the bellows is fastened to the flange seat on the interferometer enclosure, shown adjacent to the ruler in Fig. 19. The other end is attached to a window mount, which is secured in turn to the carriage. This window mount is shown in Fig. 21 with the tooling used to bond the window to the end facing the straightedge.
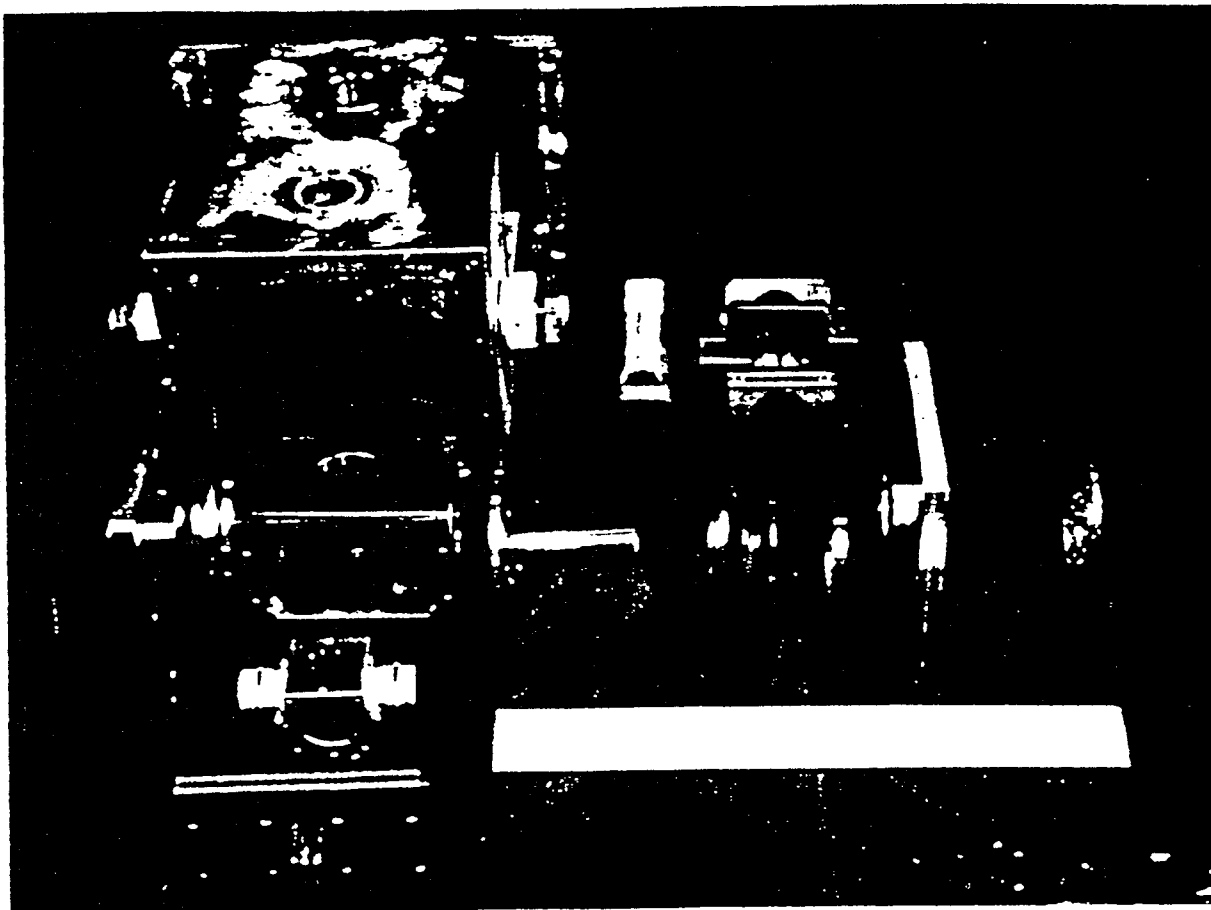
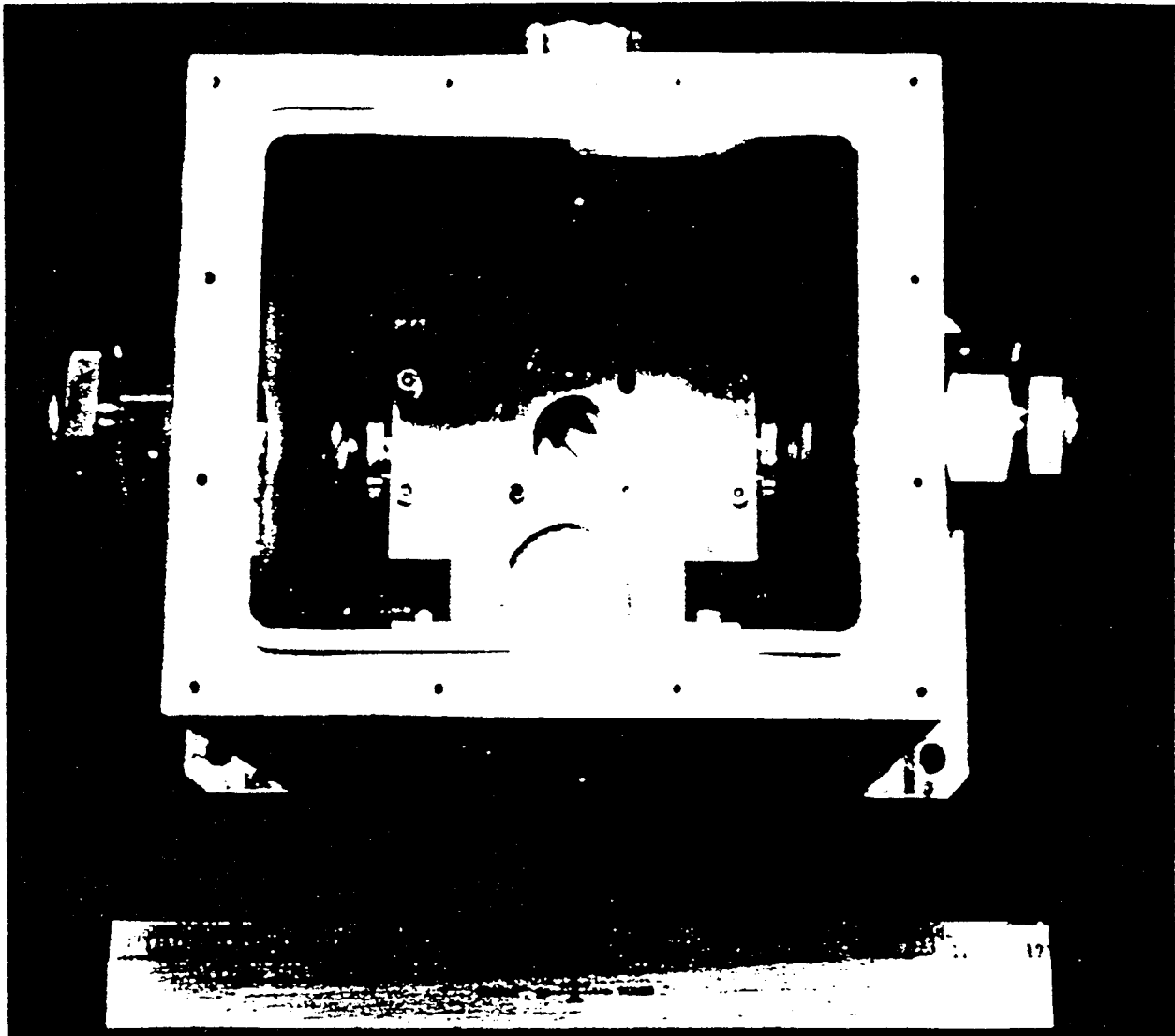Figure 3.18   A view of a partially assembled X-axis interferometer.

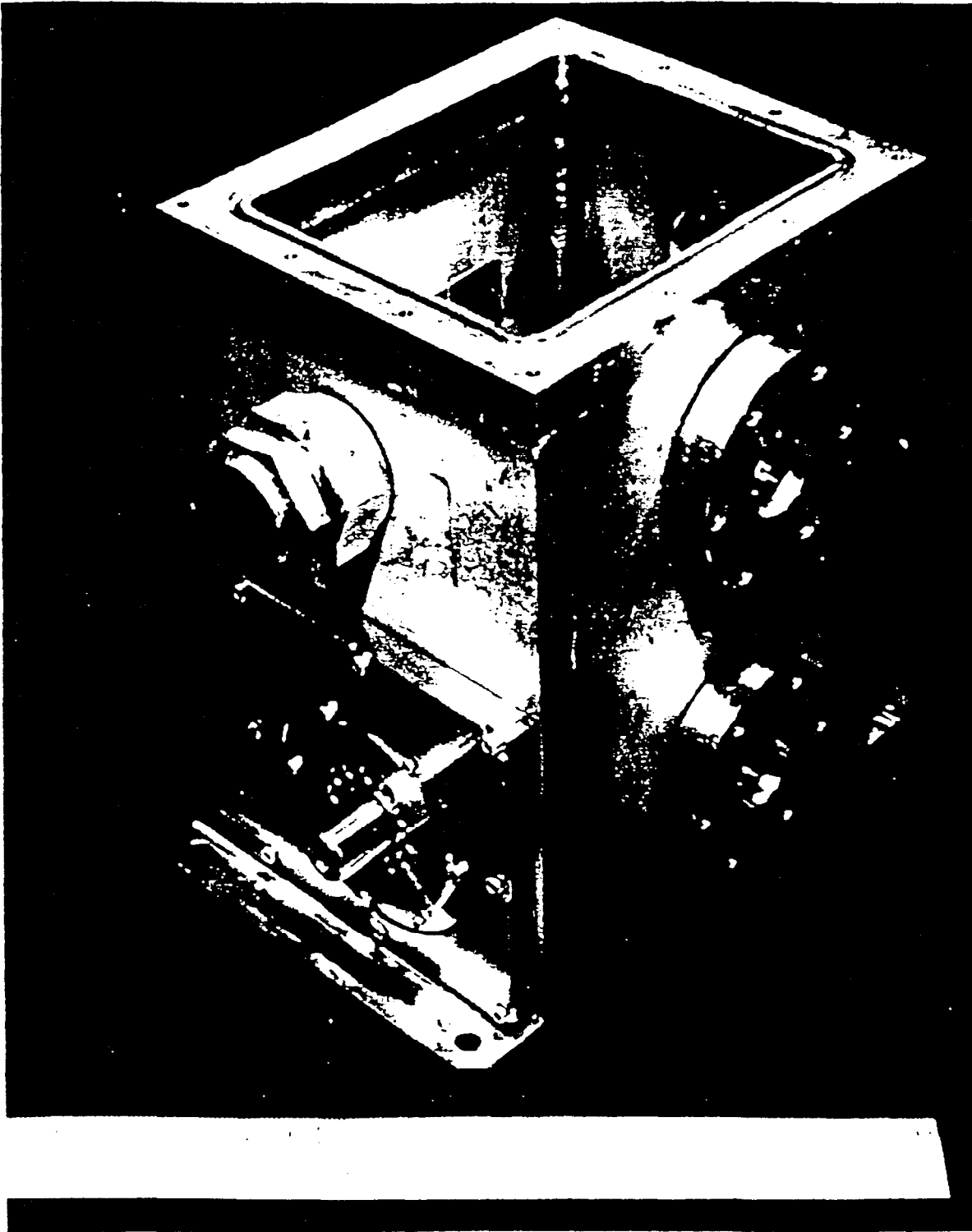Figure 3.19    Top view of an X-axis interferometer.

Figure 3.20    X-axis interferometer assembly (minus cover) showing
the mounting shaft.

With this design, all forces generated by extending or compressing the bellows are transmitted directly to the interferometer vacuum enclosure, which is bolted to the main frame of the machine. Thus, the interferometer and its mounting are isolated from all forces originating from carriage movement or main frame deflection, except for some small torsional moments that can be transmitted through the vacuum-seal boots. These torsional moments have no measurable effect on the apparent X position of the interferometers, relative to the toolbar.

### 2.6.3 Z-axis Interferometer

A Z-axis interferometer assembly is shown in Fig. 22. It consists of a rectangular vacuum enclosure, an inner frame (shown in phantom) for mounting three interferometers, three enclosure extensions at the bottom, and three H-P interferometer receivers mounted on the top cover.

The two outer enclosure extensions are stainless-steel tubes terminated by a glass window at the bottom. These outer extensions each contain two interferometer measurement arm beams that "look at" the reflective surface of a horizontal straightedge mounted on the metrology frame. One of the straightedges is mounted on each side of the carriage. The center extension is a stainless-steel bellows. The lower end of this bellows terminates at the bottom of the toolbar, just below the tool-bar mirror. The center interferometer measurement beams "look at" this mirror.

The laser beam paths through the Z-axis interferometer assembly are shown in Fig. 23. An orthogonally polarized beam enters through the window at the top left. It is turned 90° by a plane mirror, and directed horizontally through two beamsplitters to another plane mirror located at the far right of the interferometer frame. Only the upper halves of the beamsplitters and the right-hand mirror have reflective coatings. This allows the combined reference and measurement arm beams to be transmitted upward through the beamsplitter/mirror substrates and the window to the H-P interferometer receiver (mounted on the top cover of the enclosure).

Details of the interferometer mounting frame are shown in Figs. 24 to 26. The frame (Figs. 24 and 25) is a machined weldment made from superinvar. It was carefully stress relieved and heat treated to give good long-term dimensional stability. The

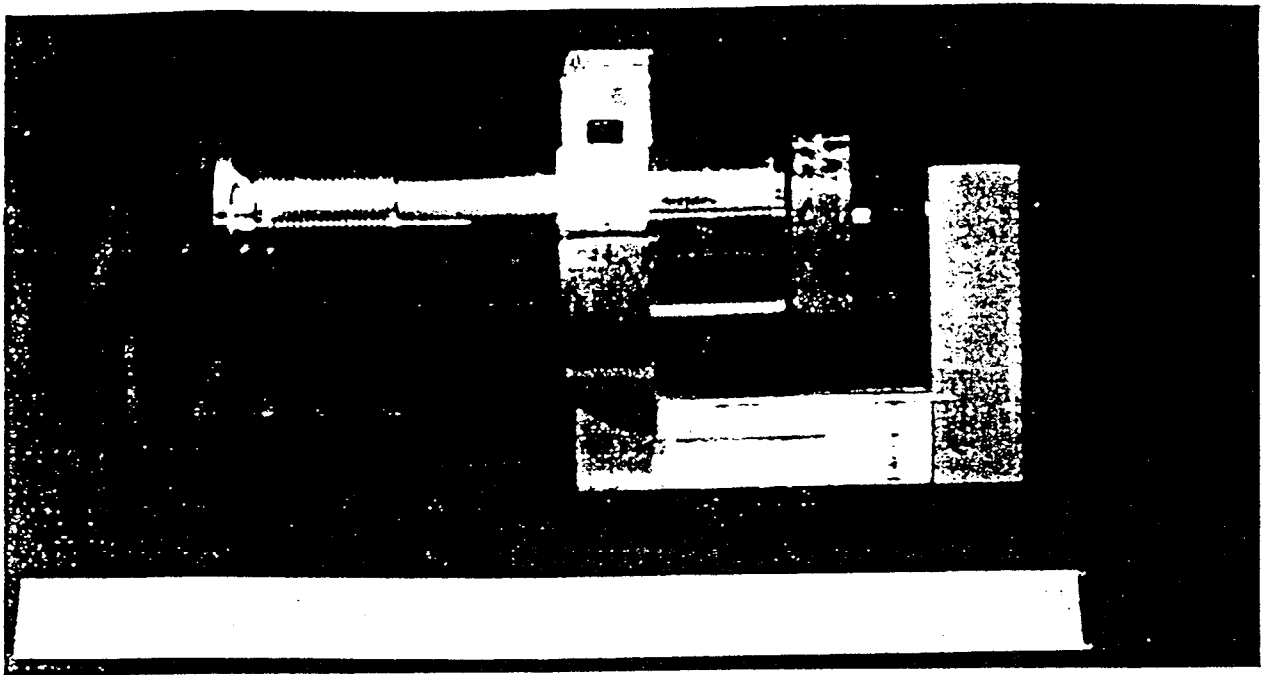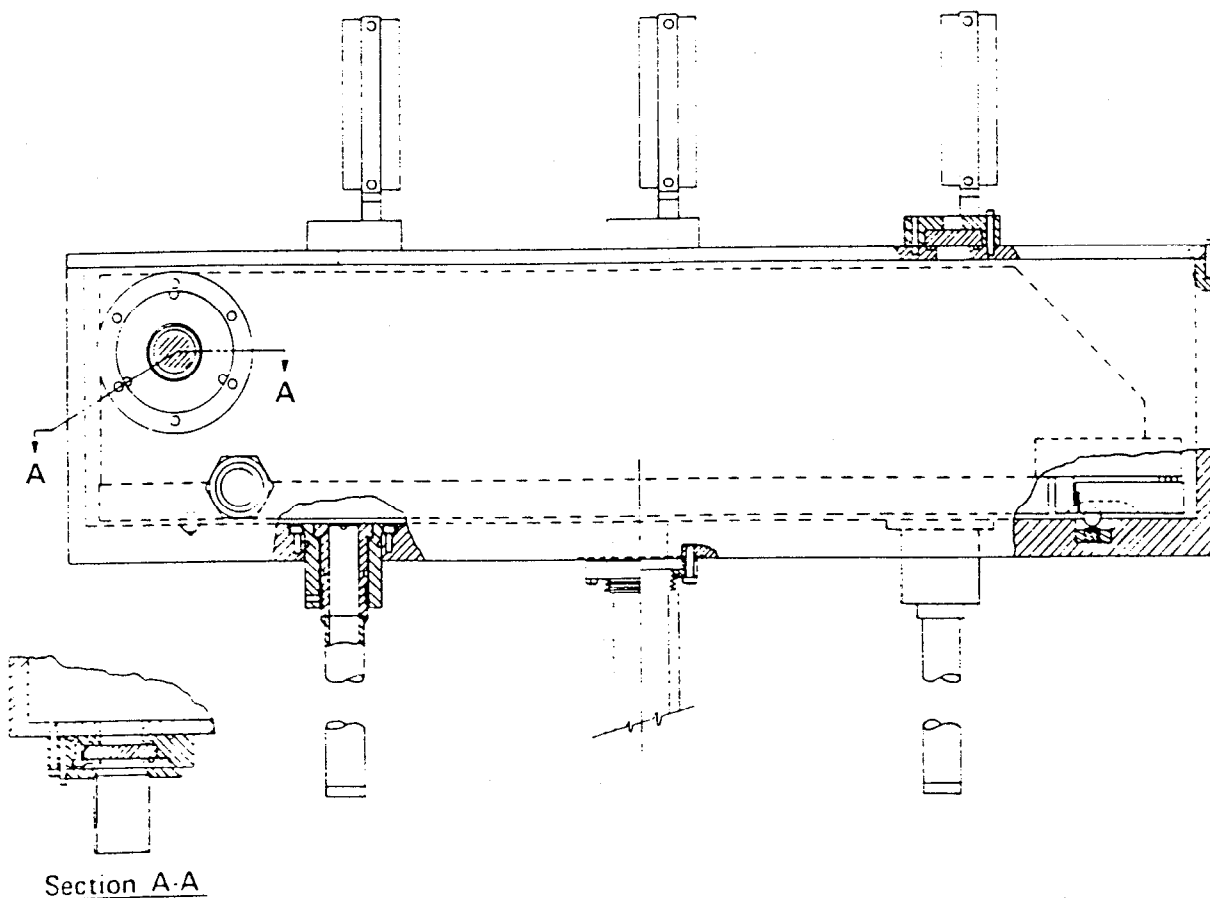Figure 3.21   X-axis interferometer window mount and the special tooling used to install window.



Section A·A

Figure 3.22   Exterior view of the Z-axis interferometer assembly, with a cross-sectional view of the beam window and mount.
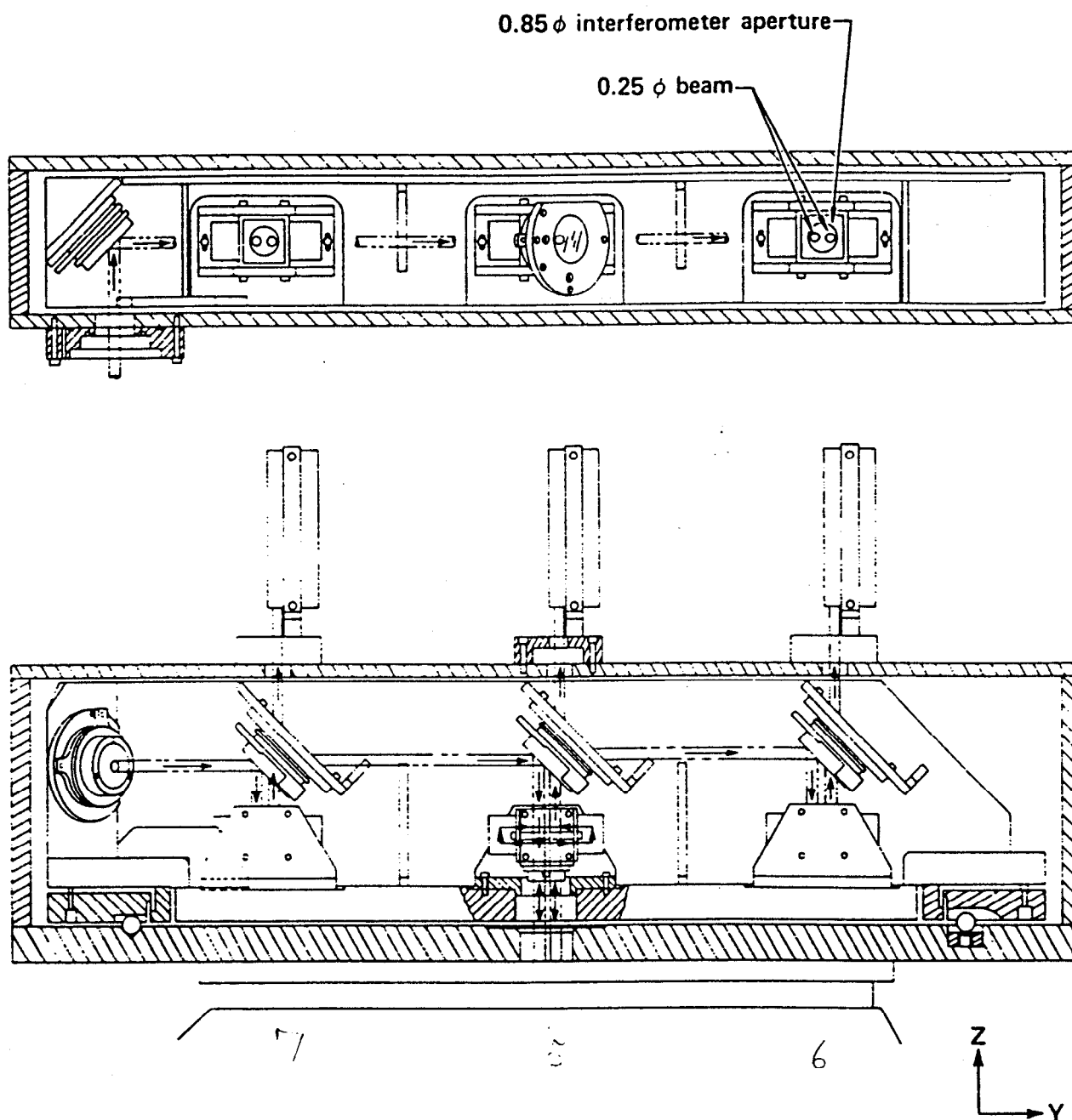
0.85 φ interferometer aperture

0.25 φ beam

Z

Y

Figure 3.23   Top and side views showing the internal layout of the Z-axis interferometer assembly and the laser beam paths through it.

frame is kinematically mounted to the bottom of the vacuum enclosure, which in turn is bolted to the top surface of the carriage.

The kinematic mount that is used is a traditional design combination of cone, flat, and V-groove. The upper half of each of the mounts is supported by an adjustable flexure (see lower left of Fig. 24). The flexure is made from 18% Nickel maraging steel heat treated to provide a yield stress of well over 200,000 psi. At maximum deflection, the flexures are stressed only to 15% of their yield stress. This assures good long-term dimensional stability. The adjustable flexures allow the interferometer frame to be aligned parallel to the top of the horizontal straightedges mounted on the metrology frame.

All beamsplitters and mirrors are mounted in holders (Dwg. 81-103592) specially designed and fabricated for the LODTM interferometer system. A close-up view of one of these holders with the optic retaining spring is shown in Fig. 26. Figure 27 shows the holder as used in the Beam Modulator Assembly.

The holder provides two axes of orthogonal angular adjustment over a range of ± 10 milliradians. The minimum increment of angular adjustment is about 20 μradians (4 sec of arc). The same maraging steel and heat treatment as is used for the holders is used for the adjustable flexures. There are a total of 21 of these holders on the LODTM. They are used in the Z-axis interferometer assembly and in the beam transfer system, described in the next section.

## 2.6.4 The Beam Transfer System

As stated in Sec. 2.3, the Beam Transfer System takes the single output beam from the beam modulator, divides it into seven equal-intensity beams, and directs these beams to the seven individual interferometers.

Figure 27 shows the mounted beam turning mirror at the outlet of the Beam Modulator Assembly. The 45° bracket supporting the mirror mount shows the construction typically used for all of the optic mount supports in the Beam Transfer System. These supports are machined weldments made from type 304 stainless steel. Mounting surfaces were machined flat to within 0.005 in with a 63 μin A-A surface roughness.
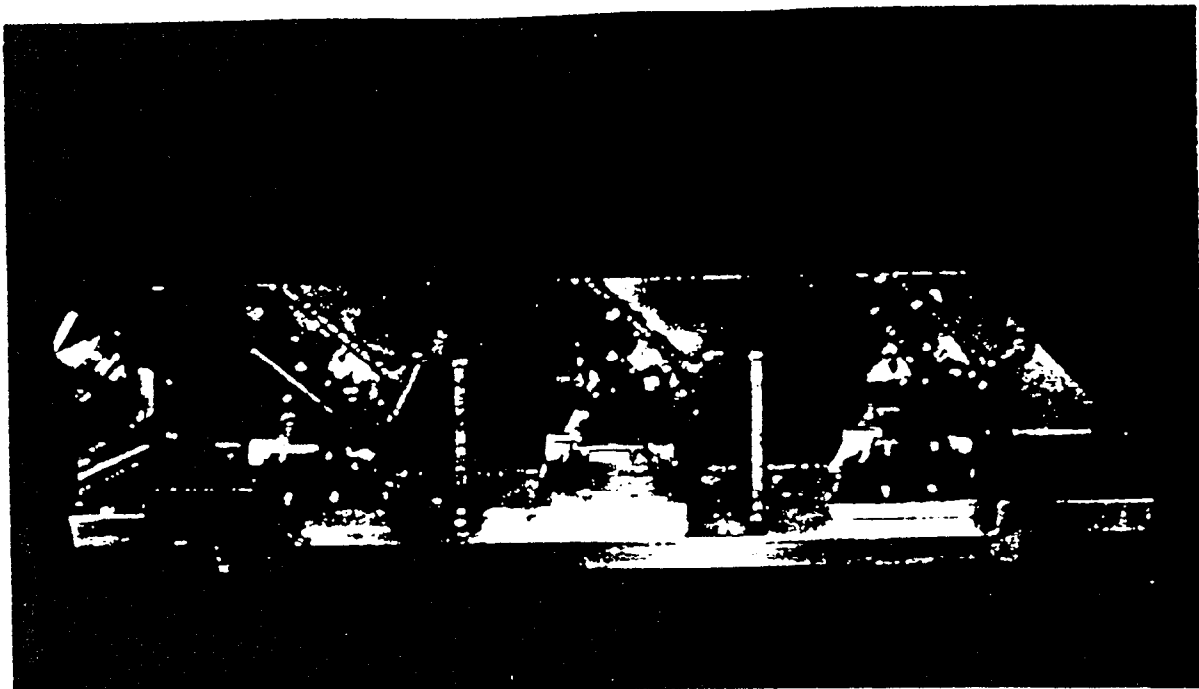
Figure 3.24    The kinematic mounting frame for the Z-axis
interferometer.



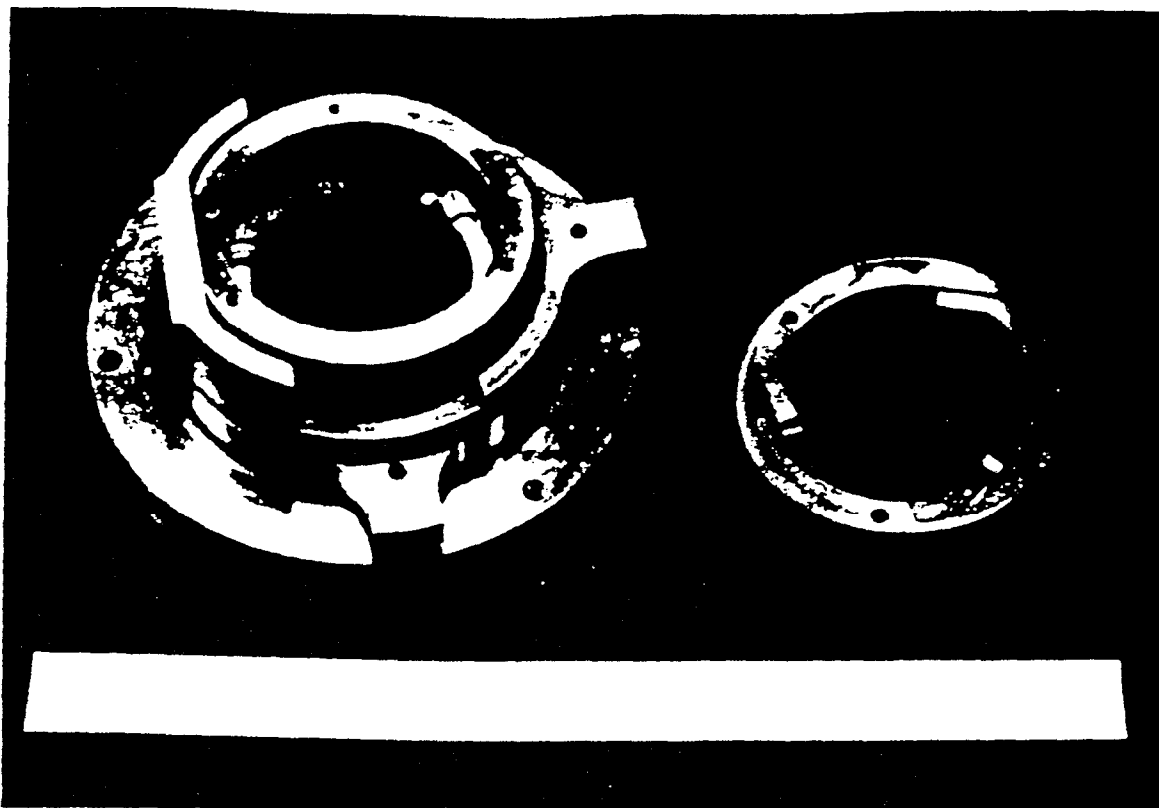Figure 3.25    Close-up view of a beamsplitter mount in the Z-axis
interferometer.

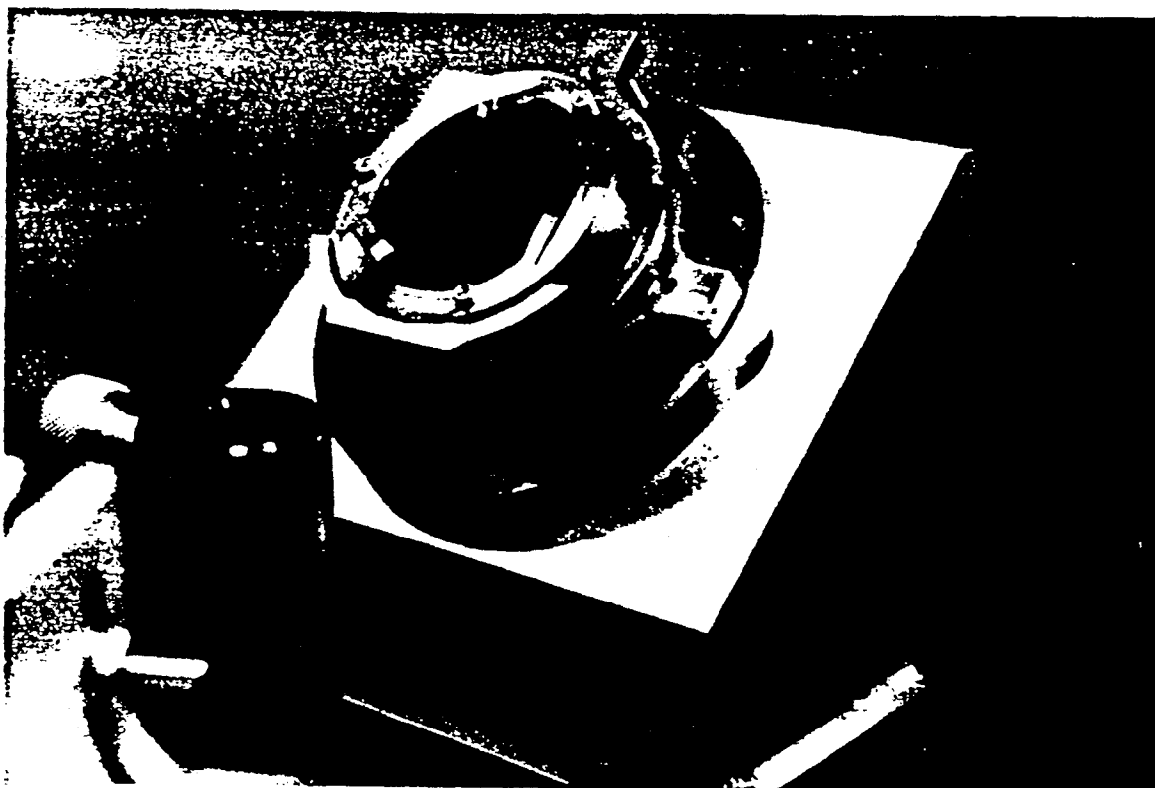Figure 3.26   An unassembled optics holder, as used in the Z-axis interferometer.



Figure 3.27   An assempled optics holder mounted on the beam modulator assembly.

The two major subassemblies of the Beam Transfer System are shown in Figs. 28 and 29. The beamsplitters and mirrors that divide the single supply beam and distribute it to the various interferometers are mounted on these units. The large platforms shown in Figs. 28 and 29 are 3/8 in thick weldments made from type 304 stainless steel. Mounting surfaces were finished-ground with a surface roughness of 32 $\mu$in A-A.

Both of these subassemblies were preassembled and pre-aligned using a surface plate and an auto collimator, before installation on LODTM. Only minor adjustments of the optics holders were required for final system alignment after mounting on the machine.

The spool-shaped part in the center of the unit shown in Fig. 28 is a center support for a cover. Both covers are weldments made from 1/8 in thick aluminum.

## 2.7 Laser Source

The laser source consists of two major components: a frequency-stabilized He-Ne laser and a beam modulator assembly. These components, depicted schematically in Fig. 30a, supply the interferometer system with a collimated 10 to 30 mW beam of laser light suitable for heterodyne interferometry, with a 1.75 MHz frequency difference between the vertically and horizontally polarized components. The wavelength stability of the beam must be on the order of 1 part in $10^9$.

Wavelength stability is obtained by using a small, low-powered reference laser. For the highest accuracy, an iodine-stabilized laser (based on the design developed at the National Bureau of Standards in Gaithersburg[9], Md.) has been used. For much of the LODTM operation, a Zeeman-stabilized laser was used (H-P model 5518A). While its long-term stability is considerably inferior to that of an iodine-stabilized laser, its short-term stability is adequate for most operations, and it is less sensitive to vibration than the iodine-stabilized laser.

To supply sufficient power to the interferometer system, a Spectra-Physics Model 125 He-Ne laser with a cavity extension was used. This laser can produce more than 50 mW of multi-mode power. Because precise wavelength control and a long coherence length are needed in the interferometers, the laser is restricted to a single axial mode
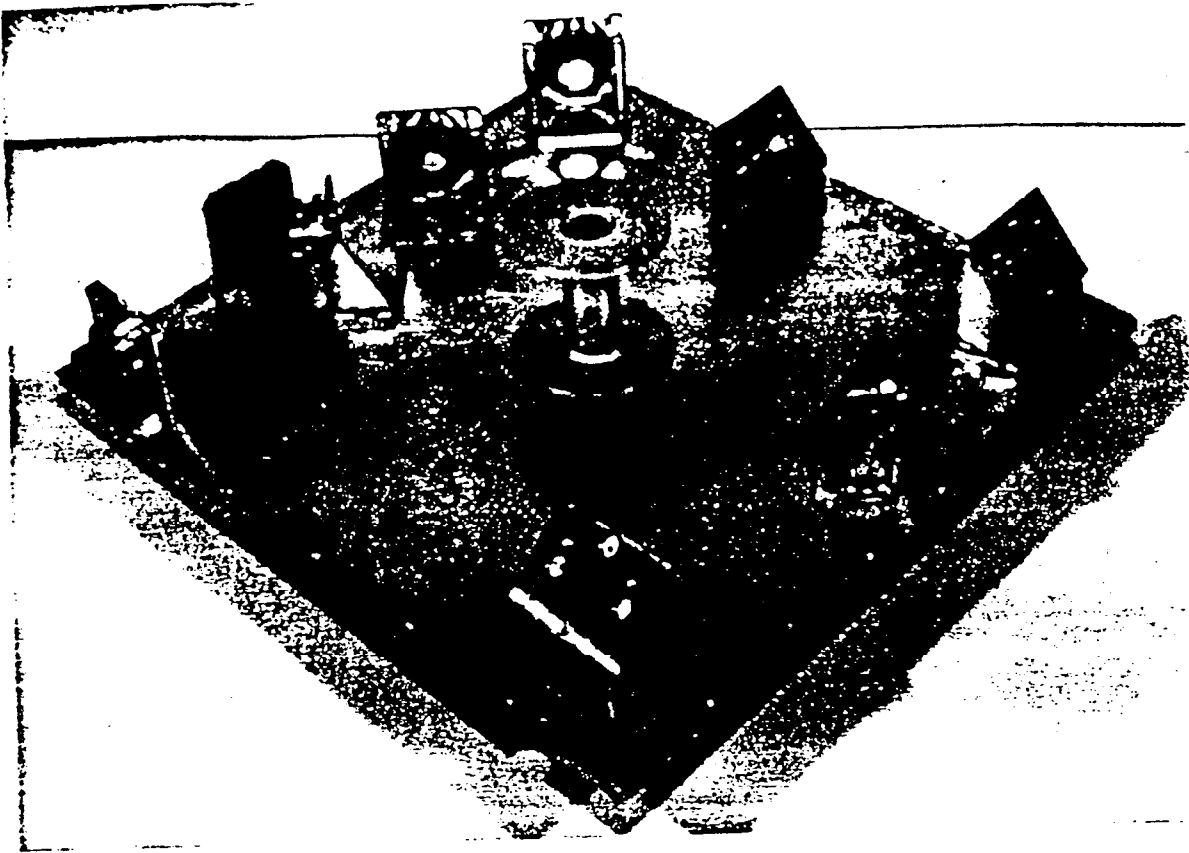
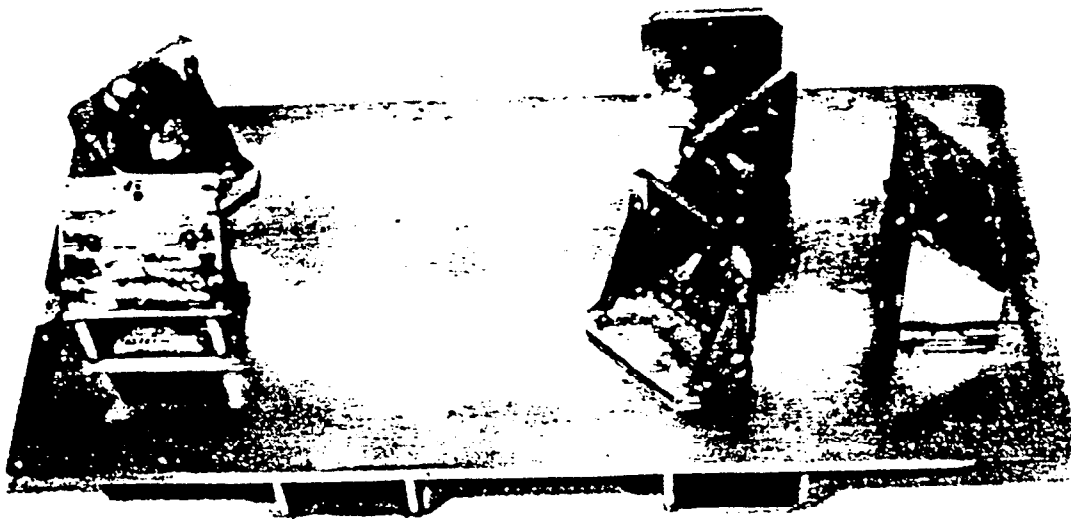Figure 3.28    The north side beam-transfer assembly.



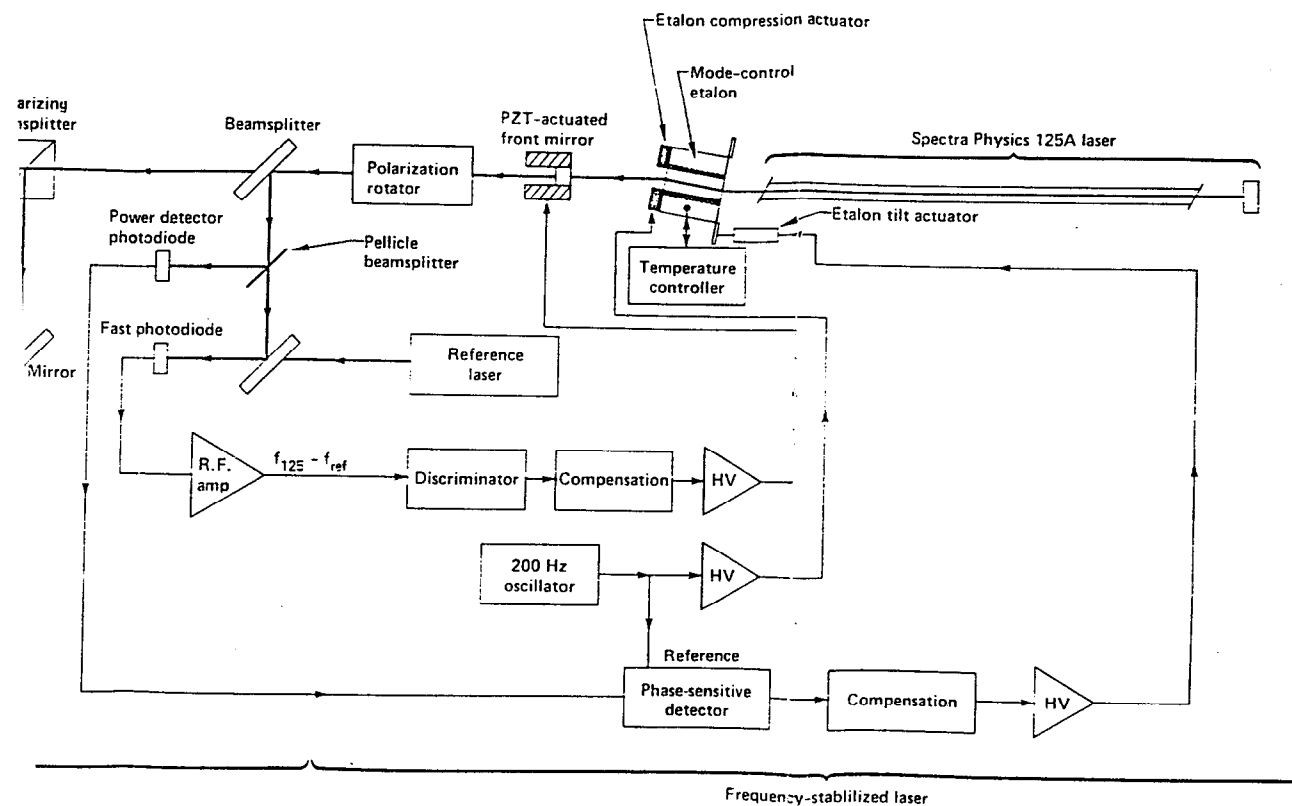Figure 3.29    The south side beam-transfer assembly.

by adding an etalon to the system[10,11]. The etalon used here is of a 2 in length of fused silica with 30% reflective dielectric coatings on each end.

The lasing wavelength of the SP-125 laser is controlled by adjusting both the tilt of the intracavity etalon and the position of the front mirror. The intracavity etalon selects an appropriate portion of the laser gain profile, and the front mirror position adjusts the exact cavity length for fine control of the wavelength. The output of the SP-125 and the reference laser are mixed in a fast avalanche photodiode to provide an RF signal with a frequency equal to the difference between the optical frequencies of the two lasers. This RF signal is applied to a frequency discriminator to produce a level that is proportional to the difference between the RF signal frequency and the desired frequency-offset lock point (30 MHz). This level is then used to close a servo-control loop with the SP-125 laser front mirror.

To obtain maximum power, and to prevent a jump of axial mode with a resulting unlocking of the wavelength stabilization system, the intracavity etalon tilt must be actively controlled. This is done with two systems: a temperature control system that prevents major thermal drift in the etalon's length, and an active system that peaks output power by adjusting the etalon tilt. The temperature control consists of a layer of constantin wire wrapped around the etalon to serve as a heater, and a thermistor bonded to its surface. The temperature of the thermistor is maintained about 1° above ambient by adjusting the power dissipation in the heater.

The power optimization servo system is implemented by introducing a small amount of dither in the length of the etalon. This is done by compressing the etalon with a piezoelectric actuator driven by an oscillator. By detecting the resulting small AC component of the measured beam power, the need for increasing or decreasing the effective path length through the etalon can be determined. Changing the etalon tilt with another piezoelectric actuator changes the effective path length.

The beam-modulator assembly (Figs. 30a and 30b) introduces the desired 1.75 MHz frequency difference between the vertically and horizontally polarized beam components. To do this, accousto-optic modulators with different frequencies are placed in the two legs of a Mach-Zehnder interferometer, which is formed by using polarizing beamsplitters[12]. A polarization rotator placed between the SP-125 laser and the beam modulator assembly provides the vertical and horizontal components for

Etalon compression actuator

Mode-control etalon

arizing splitter

Beamsplitter

PZT-actuated front mirror

Spectra Physics 125A laser

Polarization rotator

Etalon tilt actuator

Power detector photodiode

Pellicle beamsplitter

Temperature controller

Mirror

Fast photodiode

Reference laser

R.F. amp

$f_{125} - f_{ref}$

Discriminator

Compensation

HV

200 Hz oscillator

HV

Reference

Phase-sensitive detector
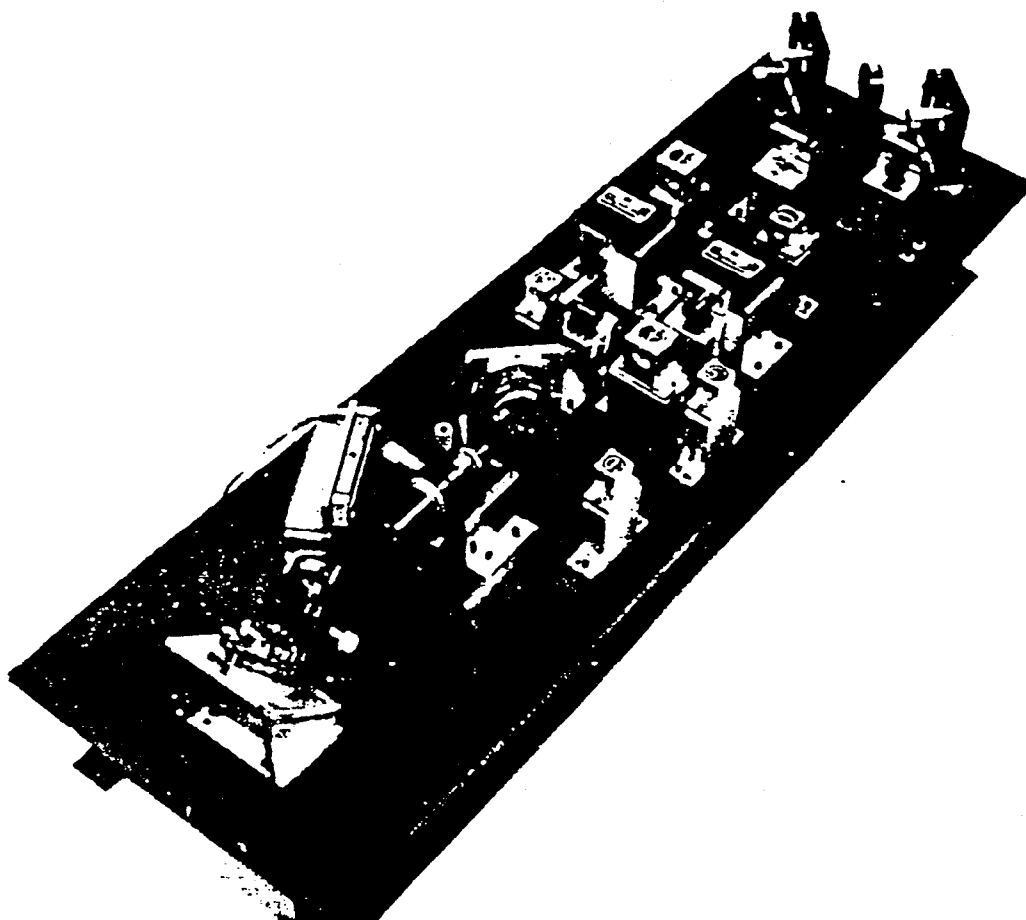
Compensation

HV

Frequency-stablilized laser

Figure 3.30b  The beam modulator assembly.

the modulator. A carrier frequency of 60 MHz was chosen, so that any retro-reflected beam would be shifted to a frequency of minimum gain in the laser. This prevents such reflections from perturbing the laser output.

The beam exiting the Mach-Zehnder interferometer is spatially filtered and expanded to a nominal 6 mm diameter before being used by the interferometer system. With the exception of beam power and wavelength stability, this 6 mm beam is essentially the same as that supplied by a Hewlett-Packard Model 5518 laser head, so standard H-P interferometer components can be used in the system.

## 2.8 Digital Interfaces

All interferometers used in the LODTM metrology system are "plane mirror" Michelson interferometers, and have two passes of the optical beam in the measurement leg. Thus, the signal at the heterodyne detector has a sensitivity of one-quarter wave (about 6 $\mu$in) for each $2\pi$ of phase change relative to the reference. However, the LODTM needs to have a 0.025 $\mu$in resolution, or $\lambda/1024$. This is achieved by using laser interferometer extension electronics, which gives a phase resolution of $\pi/128$.

The electronics accepts the measurement and reference signals and generates up and down pulses corresponding to incremental position changes of 1/256 of a cycle of phase change. These up and down pulses are accumulated in a reversible counter connected to the sensor data interface for the PE 3220 computer.

Although the extension electronics provide a very high position resolution, its method of operation limits the maximum velocity. The theoretical limit for any type of instrumentation is reached when the Doppler shift in the measurement leg equals the 1.75 MHz frequency separation of the two beams; this occurs at a velocity of approximately 10 in/sec. The laser extension electronics provide an actual limit of approximately 0.16 in/sec or 9.6 in/min maximum axis velocity.

# References

1.  A. E. Siegman, "The Antenna Properties of Optical Heterodyne Receivers," Proc. IEEE, Vol 54, No. 10, p. 1350, Oct. 1966.

2.  O. E. De Lange, "Optical Heterdoyne Detection," IEEE Spectrum, p. 77, Oct. 1968.

3.  R. Crane, "Interference Phase Measurement," Appl. Optics, Vol. 8, No. 3, p. 538, March 1969.

4.  J. N. Dukes, and G. B. Gordon, "A Two-Hundred-Foot Yardstick with Graduations Every Microinch," The Hewlett-Packard Journal, Aug. 1970.

5.  R. Baldwin, G. B. Gordon, and A. F. Rud, "Remote Laser Interferometry," The Hewlett-Packard Journal, December 1971.

6.  R. R. Donaldson, "Large Optics Diamond Turning Machine, Vol. I, Final Report", UCRL-52812, Lawrence Livermore National Laboratory, Livermore, CA, Sept. 1979.

7.  W. T. Estler, "High-Accuracy Displacement Interferometry in Air," Applied Optics, Vol. 24, No. 6, pp. 808-815, March 15, 1985.

8.  W. T. Estler, "Calibration and Use of Optical Straightedges in Metrology of Precision Machines", Optical Engineering, Vol. 24, No. 3, pp. 372-379, May/June 1985.

9.  H. P. Layer, "A Portable Iodine Stablized Helium-Neon Laser," IEEE Transactions on Instrumentation and Measurement, IM-19, Dec. 1980.

10. H. P. Barber, "Coherence Length Extension of He-Ne Lasers," Applied Optics, Vol. 7, No. 3, p. 559, March 1968.

11. M. Hercher, "Tunable Single-Mode Operation of Gas Lasers Using Intracavity Tilted Etalons," Applied Optics, Vol. 8, No. 6, p. 1133, June 1969.

12. N. A. Massie, R. D. Nelson, and S. Holly, "High-performance Real-time Heterodyne Interferometry," Applied Optics, Vol. 18, No. 11, p. 1797, June 1, 1979.

# Appendix A

## Polarization Mixing Error in
## a Heterodyne Interferometer

The heterodyne interferometer used for distance measuring on the LODTM is subject to errors introduced by the inadvertent mixing of undesired polarization components in the reference and measurement legs. The basic interferometer is shown in Fig. A-1. The two orthogonally polarized, frequency split beams from a HeNe laser have frequencies $v_1$ and $v_2$. These spatially superposed beams are incident on a polarizing beamsplitter. Beam 2 at frequency $v_2$ is S polarized and reflects from the coating up to the attached corner cube. This beam is returned to the beam splitter to be reflected into the detector, as shown. This forms the reference leg of the interferometer. Beam 1 at frequency $v_1$ is P polarized and is transmitted by the beamsplitter through a quarter-wave plate. This quarter-wave plate converts the linearly polarized beam into a circularly polarized beam, which reflects and changes handedness at the plane mirror in the measurement leg. The returning beam is converted to S polarization by the quarter-wave plate before entering the beamsplitter. This S polarized beam is reflected down to another corner cube mounted on the beamsplitter, and is returned to be reflected back through the measurement leg again for doubled sensistivity, plus cancellation of angular alignment errors.

The final transit through the measurement leg results in a P polarized beam at frequency $v_1$ being transmitted by the beamsplitter to the detector. Thus, we have two orthogonally polarized beams at frequencies $v_1$ and $v_2$, which are caused to interfere with one another at the detector by a polarizer rotated 45° with respect to the polarizations of the incident beams. Phase detection of the resulting AC signal yields an output that is proportional to distance variations in the measurement leg.

The foregoing description of the nominal operation of the heterodyne interferometer has completely ignored the possible presence of undesired beams in this device. This analysis assumes that all air/glass interfaces have been properly antireflection (AR) coated, so that no additional beams arise from spurious reflections.

The principal causes of polarization mixing in this interferometer are non-orthogonality of the two beams and misalignment of the beams with respect to the polarizing
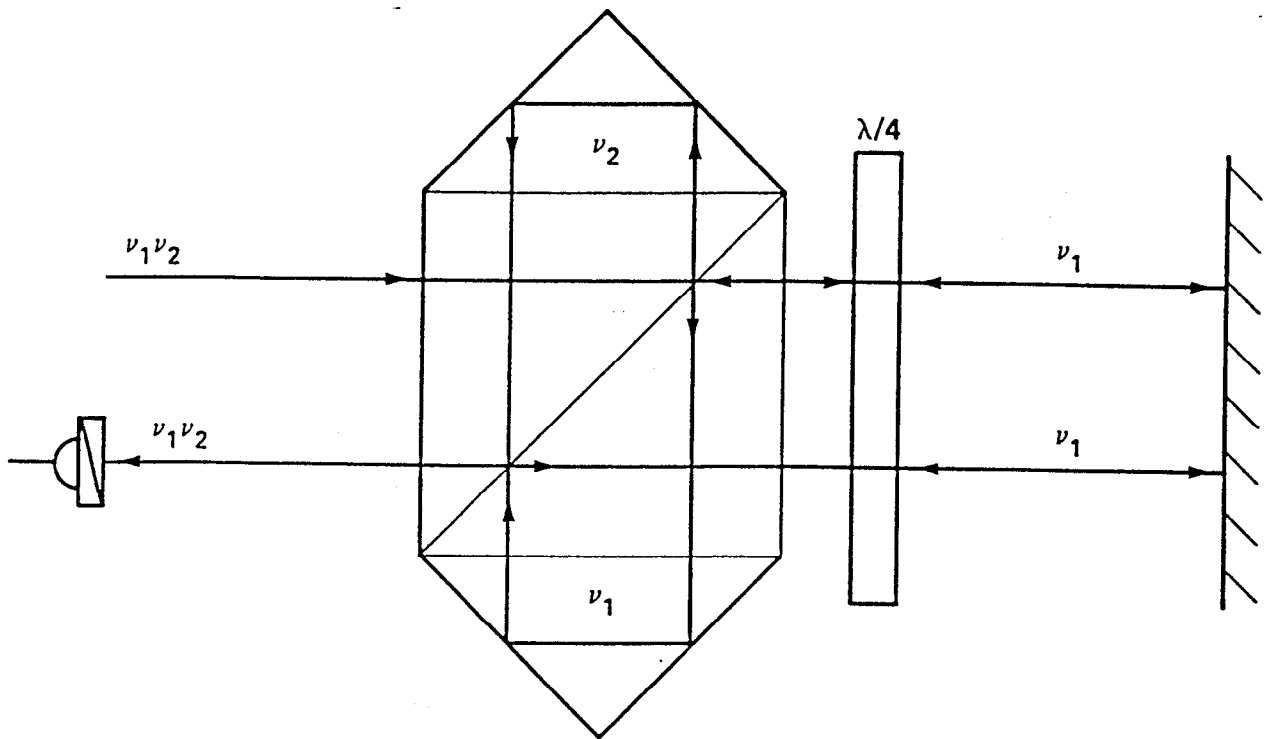
Figure A-1    A heterodyne interferometer.

beamsplitter. Polarization mixing due to an imperfect polarizing beamsplitter is relatively unimportant, because these signals do not arrive directly at the output detector.

In the following derivation, it is assumed that an undesired signal of amplitude $A_1$ and frequency $\omega_1 = 2\pi\upsilon_1$ is introduced into the measurement leg of the interferometer. In addition, an undesired signal of amplitude $A_2$ and frequency $\omega_2 = 2\pi\upsilon_2$ is introduced into the reference leg of the interferometer. This results in the presence of four fields at the output detector:

$$V_1 = (1-A_1)^{1/2} \exp i\,[k_1\,z_m - \omega_1 t + \theta_1 + \theta_{m,1}]$$

$$V_2 = A_2 \exp i\,[k_2\,z_m - \omega_2 t + \theta_2 + \theta_{m,2}]$$

$$V_3 = (1-A_2{}^2)^{1/2} \exp i\,[k_2\,z_r - \omega_2 t + \theta_2 + \theta_{r,2}]$$

$$V_4 = A_1 \exp i\,[k_1\,z_r - \omega_1 t + \theta_1 + \theta_{r,1}]$$

where k is the wavenumber $(2\pi/\lambda)$, $z_r$ is the optical path distance traveled by the beams in the reference leg and $z_m$ is the optical path distance traveled by the beams in the measurement leg. The fixed arbitrary phases of the initial laser beams are represented by $\theta_1$ and $\theta_2$. The net phase shift of a beam traversing the measurement leg is represented by $\theta_{m,j}$, and that of a beam traversing the reference leg by $\theta_{r,j}$. The j subscript on these net phase shifts accounts for the dispersion in phase between the two frequencies of beams 1 and 2. This dispersion is ignored in the remainder of this derivation.

The fields represented by $V_1$ and $V_2$ have identical linear polarization, whereas fields $V_3$ and $V_4$ have identical linear polarization that is orthogonal to that of $V_1$ and $V_2$. A linear polarizer whose polarization axis is at 45° with respect to both of these polarization directions is placed in front of the detector to project components of all voltages in a common direction. The multiplicative factor of $1/\sqrt{2}$ common to all of the voltages at the detector, due to this projection, is ignored.

The intensity of the signal at the detector is obtained by summing the four fields and multiplying by the complex conjugate:

$$S = (V_1 + V_2 + V_3 + V_4)(V_1^* + V_2^* + V_3^* + V_4^*)$$

The result is six DC terms and four AC terms. The DC terms are not detected by the AC coupled phase detector, and thus will be ignored. The four AC terms all have a frequency $\Delta\omega = \omega_2 - \omega_1$. The position information in the interferometer is carried in the phase of the AC signal. This phase, $\theta$, may be calculated as:

$$\theta = -\tan^{-1}\frac{\int S\sin(\Delta\omega)dt}{\int S\cos(\Delta\omega)dt} = -\tan^{-1}\frac{Q}{I}$$

where the integration is carried out over one period of $\cos(\Delta\omega t)$. The integrals Q and I may be readily evaluated analytically to yield:

$$\frac{I\Delta\omega}{\Pi} = \left(1 - A_1^2\right)^{1/2}\left(1 - A_2^2\right)^{1/2}\cos\left(\Delta k z_r - k_1 z_d + \Delta\theta - \varphi\right)$$

$$+ A_2(1-A_1^2)^{1/2}\cos(\Delta k z_r + \Delta k z_d + \Delta\theta)$$

$$+ A_1(1-A_2^2)^{1/2}\cos(\Delta k z_r + \Delta\theta)$$

$$+ A_1 A_2\cos(\Delta k z_r + \Delta k_2 z_d + \Delta\theta + \varphi)$$

$$\frac{Q\Delta\omega}{\Pi} = \left(1 - A_1^2\right)^{1/2}\left(1 - A_2^2\right)^{1/2}\sin\left(\Delta k z_r - k_1 z_d + \Delta\theta - \varphi\right)$$

$$+ A_2(1-A_1^2)^{1/2}\sin(\Delta k z_r + \Delta k z_d + \Delta\theta)$$

$$+ A_1(1-A_2^2)^{1/2}\sin(\Delta k z_r + \Delta\theta)$$

$$+ A_1(1-A_2^2)^{1/2}\sin(\Delta k z_r + \Delta\theta)$$

$$+ A_1 A_2\sin(k z_r + \Delta k_2 z_d + \Delta\theta + \varphi)$$

where $\varphi = \theta_m - \theta_r$, $\Delta\omega = \omega_2 - \omega_1$, and $z_d = z_m - z_r$. The apparent instrument error (in waves) will then be given by:

$$\frac{z_{error}}{\lambda} = \frac{\theta - \theta_0}{2\pi}$$

where $\theta_0$ is the phase with no polarization mixing ($A_1 = A_2 = 0$). A plot of the error for 20% mixing ($A_1^2 = A_2^2 = 0.2$) is given in Fig. A-2.
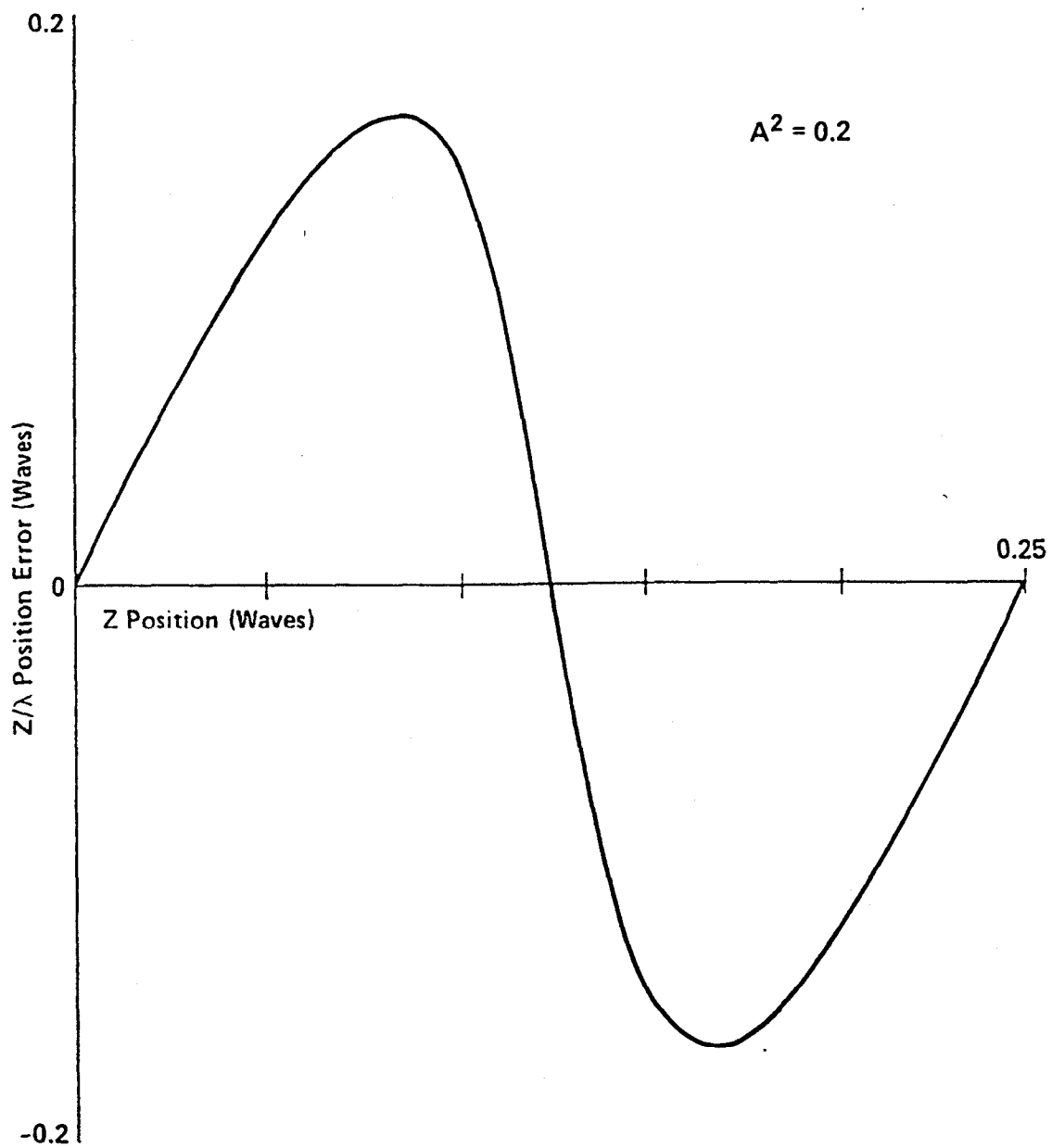
Figure A-2    Apparent position error due to 20% amplitude
polarization mixing.

# APPENDIX B

## The LODTM Interferometer System

## Performance Requirements and Design Specifications
## for Major Subsystems and Components

## 1.0 Performance Requirements for the LODTM Interferometer System

1.  Provide seven continuous positional signals in real time (updated every 1.5 msec), with four measuring horizontally in the X-Z plane, and three measuring vertically in the X-Z plane of the machine.

2.  Positional information must be resettable to zero in both the horizontal and vertical axes, relative to an arbitrary datum (tool-set station).

3.  Least count (resolution) of the interferometers shall be 1/1024 of the He-Ne laser wavelength, or 0.618 nm (0.0243 μin).

4.  The root sum of the squares of all errors, including those caused by environmental changes, shall not exceed 2.0 nm (0.080 μin) over a continuous period of 24 hours, for the full carriage travel of 44 in (X direction) and 20 in of toolbar travel (Z direction).

5.  The long-term absolute accuracy of the interferometer least count shall be known and remain constant within 1 part in $10^9$ over the lifetime of the machine.

6.  The interferometer system shall perform as specified above, while operating within the following environmental conditions:

    a)  Ambient air temperature:     $68 \pm 0.02°$ F
    b)  Ambient air humidity:        20 to 60% RH
    c)  Ambient air pressure:        760 torr $\pm$ 10%
    d)  Machine temperature:         $68 \pm 0.001°$ F

7. The interferometer shall operate within specifications for a continuous period of 10,000 hours without replacement or realignment of major subsystems on components.

## 2.0 Performance Requirements and Design Specifications for Major Subsystems and Components

### 2.1 Laser Light Source Assembly

### 2.1.1 Performance

1. The system shall produce two collinear, orthogonally polarized, visible wavelength beams, having a combined continuous-wave power of at least 4 mW.

2. Beams shall be modulated at a difference frequency of 1.75 MHz.

3. The exit-beam diameter shall be 0.25 in and the beam divergence shall not exceed 0.24 milliradians.

4. The plane of polarization of the two beams shall be orthogonal to within ±2 minutes of arc.

5. The beams shall be collinear to within ±50 microradians.

6. The system shall provide a common phase reference signal for all seven interferometers.

7. The beams shall have a coherence length of at least 40 meters (i.e., the frequency bandwidth of laser emission must be about 7.5 MHz or less), to accommodate unequal interferometer path lengths of up to 10 meters.

## 2.1.2  Component Specifications

## 2.1.2.1  Iodine-Stabilized, Helium-Neon Laser

Output Wavelengths and Frequencies:

| Line | Vacuum Wavelength (nm) | Frequency (Hz x $10^{14}$) |
|------|------------------------|----------------------------|
| d | 632.991 178 | 4.73612 380 |
| e | 632.991 196 | 4.73612 366 |
| f | 632.991 213 | 4.73612 353 |
| g | 632.991 231 | 4.73612 340 |
| h | 632.991 370 | 4.73612 236 |
| i | 632.991 399 | 4.73612 214 |
| j | 632.991 428 | 4.73612 192 |

Beam diameter: 1 mm (0.040 in)

Output mirror: Spectra Physics Part No. G3818-006, 60 cm radius concave, R=0.991 (0.9%T)

Rear Mirror: Spectra Physics Part No. G3801-012, plano, R=0.9996 (0.04%T)

Resonator Characteristics:
  Transverse Mode: $\text{TEM}_{00}$

  Resonator Configuration: Long radius

  Longitudinal Modes: Single axial mode

  Cavity length: 37.1 cm (14.6 in)

  Axial-mode spacing: 404 MHz

  Plasma excitation: D.C., 5 to 6 ma @ 1.5 KV

  Beam-amplitude noise: <0.2% rms, <0.5% P-P

  Current regulation: ±0.05 ma

Power requirements:
  Voltage: 115/230 VAC ±10%

  Power: 17 Watts

Long-term frequency stability: 3 parts in $10^{10}$

Uncertainty in output wavelength or frequency: 1 part in $10^9$

## 2.1.2.2 Spectra-Physics Model 125A Helium-Neon Laser

The laser manufacturer's specifications are summarized as follows:

Output wavelength: 632.8 nm in air; 632.991 nm in vacuo

Beam diameter: 1.8 mm (0.072 in) @ $1/e^2$

Beam divergence: 0.6 milliradian

Output mirror: Part No. G3814-001, 6 meter radius concave, R=0.974

Rear Mirror: Part No. G005-003, Brewster-angle prism-flat, R=0.997.

Resonator Characteristics:

Transverse mode: $TEM_{00}$

Degree of polarization: $1 \times 10^{-3}$

Angle of polarization: Vertical ± 5°

Resonator Configuration: Long radius

Cavity length: 2.03 m (80 in)

Axial mode spacing: 74 $MH_z$

Plasma Excitation: D.C., 25 to 35 mA @ 6KV RF; 15 watts @ 40.7 MHz

Amplitude Stability:

Beam amplitude noise: (1-100KHz) - 0.3% rms with RF excitation

Beam amplitude ripple: (1-120 Hz) - 0.5% rms with RF excitation

Long term power drift: less than 5% over 8 hours

Power Requirements:

Voltage: 115/230V ± 10%, 50-60 Hz

Physical Characteristics:

Weight: Laser head - 100 lb; Power Supply - 30 lb

Laser Head dimensions: 84 in long x 11 in high x 6.5 in wide

Coherence etalon (S.P. Dwg. No. 410-363):

Material: fused silica (i.e., Corning Code 7940, Schlieren grade)

Dimensions: 15 mm (0.59 in) dia. x 50.8 mm (2.0 in) long

Clear aperture: 10 mm (0.4 in)

Flatness of ends: ± 1/8 wavelength

Wedge angle: 1/10 wavelength, in transmission

Free spectral range (C/2nt): 2 GHz

Output Mirror PZT:
  Burleigh Model PZ-80
  Motion sensitivity: 0.006 )m/v
  Maximum Voltage: +1000v
  Linearity: $\leq 5\%$
  Maximum motion: 6 $\mu$m (240 $\mu$in)

Etalon Tilt PZT (Horizontal Plane):
  Burleigh Model PZ-44
  Motion Sensitivity: 0.04 $\mu$m/v
  Linearity: $\leq 5\%$
  Maximum motion: 40 $\mu$m (1600 $\mu$in)

Etalon Tilt Micrometer (Vertical Plane):
  Oriel Model 18231 (spherical tip, 0.5 in travel)
  Supply Voltage: 12v
  Screw Pitch: 0.485 mm (0.020 in)
  Backlash: 5 microns (0.0002 in) maximum
  Resolution: 0.02 microns

Broadband Polarization Rotator:
  Spectra Physics Model 310A
  Wavelength: 400 to 700 nm
  Extinction Ratio: $10^3$
  Clear Aperture: 8 mm (0.320 in)
  Wedge: $\leq$ 0.2 milliradian (angular difference between axes of input and output beams)
  Transmission: < 95%
  Wavefront Distortion in transmission: 1/2 wave

## 2.1.2.3   Acousto-Optic Modulators and Modulator Drivers

Acousto-Optic Modulator:
  IntraAction Corp. Model AOM-603

Center Frequency: 60.0 or 61.75 MHz

Diffraction Angle (633 nm):

$\alpha_1$ = 9.87 mr @ f = 60.00 MHz

$\alpha_2$ = 10.19 mr @ f = 61.75 MHz

Diffraction Efficiency (633 nm): 85%

Drive Power: 3.5 watts

Acousto-Optic Modulator driver:

  IntraAction Corp. Model ME-60

  Modulation Frequencies: 60.00 and 61.75 ±0.001 MHz

  RF Power Output: 2.5 to 3.2 watts

## 2.1.2.4   Other Beam-Modulator Components

Silicon Avalanche Photodiode:

  Texas Instruments Inc. Model TIED-55

  Photocurrent Gain: > 600 (typical)

  Active Area: $5 \times 10^{-4}$ cm (Dia. = 0.010 in)

  Noise-equivalent Power: $10^{12}$ w/ Hz at 1 GHz

S.P. 125 Laser Power Photodiode:

  United Detector Technology Model PIN-10 DP

  Active Area: 100 $mm^2$

  Connector: BNC Special

  Responsivity @ 850 nm: 0.50 a/w

  NEP (w/ Hz): $3 \times 10^{-13}$

  Source Resistance: 2 megohm

  Capacitance: 2400 pf at 0v

Hewlett-Packard Polarizing Beamsplitter, Beambender, and Receiver:

  Physical specifications for these components will be found in Hewlett-Packard
  Application Note 197-2, pp., 16, 17, and 24. Electronic specifications for the
  Receiver (H-P No. 10780A) will be found in H-P Operating and Service Manual
  10780A, Series 1948A.

## 2.2    Beam Transfer System

### 2.2.1    Performance

1.    The Beam Transfer System will divide the common dual-frequency, orthogonally-polarized beams into seven paths, each path to be directed to one of the interferometers.

2.    The usable* signal at each interferometer receiver shall not vary more than ± 20% from the mean signal.

3.    The minimum usable signal at any interferometer receiver shall be 50 $\mu$W for a power level of 10 mW at the exit of the Beam Modulator Assembly.

4.    The system will provide a means for angular adjustment so that the interferometer beams can be individually aligned normal to the reflective surfaces (straightedges) within ±30 microradians.

5.    The angular alignment of the beams shall not change more than ±15 microradians over a period of 8,800 hours (one year), with an ambient air temperature of 68.0 ± 0.02° F and a machine temperature of 68.0 ± 0.001° F.

6.    The phase-mixing error caused by birefringence in optical components and misalignment of the two planes of polarization of the beams shall not exceed 0.11 $\mu$in peak-to-valley (0.032 $\mu$in rms).

### 2.2.2    Component Specifications

All optical components used in the LODTM Interferometer System are shown schematically in Dwg. 81-113400, the Optics Schematic.  Physical and optical

---

* The Hewlett-Packard Corp. (H-P Tech. Note 197-2, p-34) states that the usable transmitted is proportional to the square root of the product of the transmission factors for each frequency path ($\sqrt{T_1 T_2}$).

specifications for each purchase-fabricated component are detailed on the individual drawings listed in the bill of material of Dwg. 81-113400.

## 2.3    X-Axis Interferometer System

### 2.3.1    Performance

1.    Provide four measurements of the toolbar position relative to the tool-set station in the X-Z plane

2.    The system geometry will provide carriage pitch angle information in the X-Z plane, and average any dimensional length changes of the Tool Bar or metrology frame in the X direction.

3.    The system will meet all the general requirements of Sec. 1.0.

### 2.3.2    Component Specifications

Hewlett-Packard Plane-Mirror Interferometer:
The interferometer physical specifications are given in Hewlett-Packard Application Note 197-2, p. 19. The optical performance of the polarizing beamsplitter and the corner reflector were determined from tests of a few components.

The most important functional requirement of the polarizing beamsplitter and corner reflector is that the combined polarization-mixing properties of these components be less than some reasonable limit. The overall phase mixing error was budgeted at 0.11 $\mu$in peak-to-valley, or less. This includes the mixing properties of windows, corner reflectors, polarizing beamsplitters, and interferometer angular misalignments in pitch, roll, and yaw. The polarizing beamsplitter and corner reflector (when properly mounted) accounts for about 71% of this error, on the basis of the electric-field amplitude.

Vacuum Pump and Vapor Trap:
Pump: Leybold-Heraeus, trivac, type D-16A (mechanical) Kat-Fab-Nr 89583 - 1281481016
Motor: G.E., 1 H-P, 3 phase, 60 Hz
Vapor Trap: Leybold Heraeus Adsorpte, Kat-Fab-Nr 18710

## 2.4    Z-Axis Interferometer System

### 2.4.1    Performance

1.    Provide three measurements in a vertical plane, one of the Tool Bar position, and two of the upper interferometer assembly position relative to the horizontal straightedge surfaces mounted on the metrology frame.

2.    The system will meet all the general requirements of Sec. 1.0.

### 2.4.2    Component Specifications

All component specifications for the Z-axis Interferometer are the same as for the X-axis Interferometer (Sec. 2.3.2).

## 2.5    X-Axis Detector Assembly

### 2.5.1    Performance

The X-axis Detector Assembly will provide a means of directing the combined exit beams from the interferometers into a mounted receiver.  A means of adjustment shall be provided to change the angular position of the beam in a horizontal plane, and the receiver position in a vertical plane.

### 2.5.2    Component Specifications

Right Angle Prism: 15 x 15 x 21 mm high
Material:  Commercial grade BK-7 glass
Hewlett-Packard Receiver:
  These receivers were modified for LODTM to reduce their heat output.  The +5V and +10V regulators have been removed, and the green beam-strength light has been disabled.  These voltages are provided from a central, external power supply. Maintenance instructions, schematics, and a list of replaceable parts will be found in H-P Manual Part No. 10780-90006, Operating and Service Manual for the 10780A Receiver.